

# AIR QUALITY FORECASTS ON A KILOMETER-SCALE GRID OVER COMPLEX SPANISH TERRAINS

M.T. Pay<sup>1,\*</sup>, F. Martínez<sup>1</sup>, M. Guevara<sup>1</sup>, J.M. Baldasano<sup>1,2</sup>

[1]{Earth Sciences Department, Barcelona Supercomputing Center-Centro Nacional de Supercomputación, Barcelona, Spain}

[2]{Environmental Modeling Laboratory, Technical University of Catalonia, Barcelona, Spain}

[\*]{now at: Laboratoire de Météorologie Dynamique, École Polytechnique, Palaiseau Cedex, France}

## Abstract

CALIOPE-AQFS represents the current state-of-the-art in air quality forecasting systems of high-resolution running on high-performance computing platforms. It provides a 48-h forecast of NO<sub>2</sub>, O<sub>3</sub>, SO<sub>2</sub>, PM<sub>10</sub>, PM<sub>2.5</sub>, CO, and C<sub>6</sub>H<sub>6</sub> at 4-km horizontal resolution over all of Spain, and at 1-km horizontal resolution over the most populated areas in Spain with complex terrains (Barcelona, Madrid and Andalusia domains). Increased horizontal resolution from 4 km to 1 km over the aforementioned domains leads to finer texture and more realistic concentration maps, which is justified by the increase in NO<sub>2</sub>/O<sub>3</sub> spatial correlation coefficients from 0.79/0.69 (4 km) to 0.81/0.73 (1 km). High resolution emissions using the bottom-up HERMESv2.0 model are essential for improving model performance when increasing resolution on an urban scale, but it is still insufficient. Decreasing grid spacing does not reveal the expected improvement in hourly statistics, i.e., decreasing NO<sub>2</sub> bias only by ~2 μgm<sup>-3</sup> and increasing O<sub>3</sub> bias by ~1 μgm<sup>-3</sup>. The grid effect is less pronounced for PM<sub>10</sub> because part of its mass consists of secondary aerosols, which are less affected than the locally emitted primary components by a decreasing grid size. The resolution increase has the highest impact over Barcelona, where air flow is controlled mainly by mesoscale phenomena and a lower PBL. Despite the merits and potential uses of the 1-km simulation, the limitations of current model formulations do not allow confirmation of their expected superiority close to highly urbanized areas and large emission sources. Future work should combine high grid resolution with techniques that decrease subgrid

1 variability (e.g., stochastic fields methods), and also include models that consider urban  
2 morphology and thermal parameters.

### 3 **1 Introduction**

4 The World Health Organization (WHO) has recently shown that there is sufficient  
5 evidence that particulate matter (PM), ozone (O<sub>3</sub>) and nitrogen dioxide (NO<sub>2</sub>) affect  
6 human health (WHO, 2013). Although NO<sub>2</sub> and PM concentrations improved from  
7 2002 to 2011 in Europe, the situation is still far from matching the WHO air quality  
8 guidelines (AQG). The European annual limit values for NO<sub>2</sub> (annual) and PM<sub>10</sub> (daily)  
9 had been exceeded at 42-43% of the traffic stations in 2011. For the same year, about  
10 33% of the European urban population was exposed to PM<sub>10</sub> concentrations above the  
11 daily limit value, and nearly 88% was exposed to the respective WHO AQG (EEA,  
12 2013). Air pollution legislation for the protection of the increasing city population has  
13 recently increased the demand for forecasting systems that can assess and understand air  
14 pollution dynamics, alert the population when health-related issues occur, and develop  
15 emission abatement plans (EEA, 2011).

16 When applying an air quality modeling system, defining the grid resolution is an  
17 important consideration. The potential benefits of higher-resolution modeling should be  
18 weighed against the increased complexity of the inputs, increased CPU time, and disk  
19 space requirements. In theory, higher resolution modeling is expected to yield more  
20 accurate forecasts because of better resolved model input fields (topography, land cover  
21 and emissions). Furthermore, high resolutions (ranging from 1 to 5 km) are essential to  
22 reproduce mesoscale phenomena, e.g., those controlling O<sub>3</sub> transport along the  
23 mountainous northeastern Mediterranean coast (Fay and Neunhäuserer, 2006; Jiménez  
24 et al., 2006). Even at fine scales, the modeled concentrations are not necessarily the best  
25 (Mass et al., 2002; Gego et al., 2005; Valari and Menut, 2008) because increasing  
26 emission and meteorology spatial resolution can also increase uncertainties, at the risk  
27 of reduced model performance. Nowadays, fine horizontal resolution is a persistent  
28 challenge when assessing health impacts and population exposure studies (Thompson et  
29 al., 2013).

30 Several studies have evaluated the impact of increasing horizontal resolution on  
31 different scales over the eastern and southeastern USA using the Community Multiscale  
32 Air Quality (CMAQ) model and the Comprehensive Air Quality Model with Extensions

1 (CAMx), which range from 32 km – 12 km – 4 km (Cohan et al., 2006; Tesche et al.,  
2 2006; Queen and Zhang, 2008). They found no significant changes for O<sub>3</sub> and PM (<5%  
3 on average), and those changes were even smaller at resolutions of between 12 km and  
4 4 km (<3%). Concerning PM components, Fountoukis et al. (2013) found that increased  
5 resolution provides differences mostly for primary PM rather than secondary PM.  
6 Recently, a model intercomparison exercise, named ScaleDep, was performed to  
7 determine the effect of grid resolution on air quality modeling performance over Europe  
8 at a regional and urban scale (Cuvelier et al., 2013). The exercise, involving five  
9 chemical transport models (CTMs) (EMEP, CHIMERE, CMAQ, LOTOS-EUROS and  
10 RCGC) running under the same conditions over the full year 2009 and at four  
11 resolutions (56, 28, 14, and 7 km), showed that it is difficult to define a grid size that is  
12 adequate for resolving the urban signal under all conditions affecting Europe. Still, a 14-  
13 km resolution seems to be a good compromise between background applications and  
14 those reproducing most of the urban signals (7 km resolution). However, the ScaleDep  
15 exercise did not distinguish between the different topographies or complex  
16 meteorological patterns which are characteristic of the Iberian Peninsula.

17 Few studies have been performed over selected areas in Spain; and of those, the focus  
18 has been mainly on O<sub>3</sub> and NO<sub>2</sub>. Vivanco et al. (2008) evaluated the annual impact by  
19 increasing model resolution (to 36, 19, and 7 km) over Madrid for NO<sub>2</sub> and O<sub>3</sub>. They  
20 used the WRF-CHIMERE model, disaggregating the EMEP emission inventory based  
21 on land use information. Their evaluation showed that the model improved more for  
22 NO<sub>2</sub> than O<sub>3</sub>, with the most significant improvement achieved when resolution  
23 increases from 36 to 19 km rather than to 7 km, which they linked to increased  
24 uncertainty in the emission data introduced with the disaggregation techniques. Jiménez  
25 et al. (2006) used the MM5-CMAQ model along with a bottom-up emission model  
26 (EMICAT2000) to assess the influence of grid resolution on O<sub>3</sub> (at 8, 4, and 2 km) over  
27 the complex terrain of the northeastern Iberian Peninsula (Catalonia) during a summer  
28 pollution episode. They found that both an improved performance of the mesoscale  
29 phenomena and a better allocation of emissions for the 2-km resolution improve the  
30 capability of the model to simulate exceedances of European limit values. An important  
31 issue in both studies is the emission modeling approach (top-down vs. bottom-up) when  
32 applying high resolutions at the local scale (<10 km). As Fountoukis et al. (2013) and  
33 Timmermans et al. (2013) demonstrate, in the range of local scale (e.g., the greater Paris

1 area), the grid resolution is not currently the major source of discrepancies in model  
2 performance, but instead the predicted concentrations and corresponding gradients are  
3 more consistent with observed concentrations when provided by bottom-up emission  
4 inventories rather than down-scaled inventories. If local variation in input data (e.g.,  
5 emission patterns or land use) cannot be properly characterized, modeling with a finer  
6 grid resolution may not provide any great advantages.

7 Increasing resolution is a technical challenge, since computational cost markedly  
8 increases in inverse proportion to grid spacing. The current progress in computation  
9 allows increased model resolution and for multiple spatial scales to be investigated with  
10 the aim of establishing adequate grid size for forecasting air quality at the local scale.  
11 Recently, [Colette et al. \(2014\)](#) evaluated the impact of increasing resolution up to 2 km  
12 over the European continent by using the CHIMERE model for an episode of air  
13 pollution in 2009. They simulated 2 million grid cells using over 2000 CPUs of a high  
14 performance computing system, which was hosted by the French Computing Centre for  
15 Research and Technology (CCRT/CEA).

16 In terms of computational resources, horizontal resolution is critical to an operational air  
17 quality forecast. In Europe, operational air quality systems use resolutions between 12-  
18 25 km, while applications to a single country can reach resolutions between 4-10 km  
19 ([Zhang et al., 2012](#)). Over Spain, there are three systems providing air quality forecasts  
20 running at different horizontal resolutions. The lowest resolution system is the  
21 Technical University of Madrid's OPANA (Operational Atmospheric Numerical model  
22 for urban and regional Areas), running at 27 km x 27 km and based on the  
23 MM5/CMAQ/EMIMO models ([San José et al., 2009](#)). It is followed by the Spanish  
24 meteorological office's system (AEMET,  
25 [http://www.aemet.es/es/eltiempo/prediccion/calidad\\_del\\_aire](http://www.aemet.es/es/eltiempo/prediccion/calidad_del_aire)), which forecasts at 10 km  
26 x 10 km using the HIRLAM-HRN/MOCAGE/GEMS-TNO models. The CALIOPE Air  
27 Quality Forecast System (CALIOPE-AQFS; [Baldasano et al., 2011](#); [Pay et al., 2012a](#);  
28 [and references therein](#)), of the Barcelona Supercomputing Center–Centro Nacional de  
29 Supercomputación (BSC-CNS), runs at the highest resolution, 4 km x 4 km, and it is  
30 based on the WRFv3.5/CMAQv5.0.1/HERMESv2.0/BSC-DREAM8bv2 models.  
31 Moreover, CALIOPE-AQFS provides 1-km x 1-km resolution forecasts for the Madrid  
32 and Barcelona metropolitan areas (since 2009) and the Andalusian region (since 2013).

1 Such resolution has been possible thanks to both the high performance computing  
2 resources at the BSC-CNS and the availability of detailed emission data covering Spain.

3 The present work aims to assess the impact of increasing the horizontal resolution from  
4 4 km to 1 km, specifically over areas affected by heterogeneous emission patterns and  
5 complex terrains such as the Barcelona and Madrid metropolitan areas (BCN and  
6 MAD) together with the Andalusian region (AND). For that purpose, the CALIOPE-  
7 AQFS forecasts pollutant concentrations ( $O_3$ ,  $NO_2$ , and  $PM_{10}$ ) at two horizontal  
8 resolutions: first at a 4-km resolution covering Spain (IP4), and second at a 1-km  
9 resolution covering the AND, BCN, and MAD domains. Here, a study is performed for  
10 the period April 2013, which presents a seven day air pollution episode. We use  
11 observations from routine air quality monitoring networks to evaluate both resolutions.

12 Section 2 describes the configuration and computational setup of CALIOPE-AQFS.  
13 Section 3 quantifies the impact of resolution increase on forecasting hourly  
14 concentrations (and exceedances) in terms of: pollutant, domain, building density and  
15 major emission sources. Section 4 concludes with the main results and some  
16 recommendations.

## 17 **2 Methodology**

### 18 **2.1 Domain and period under study**

19 [Figure 1](#) shows the primary  $NO_2$  emission patterns and topographic characteristics of  
20 the BCN, MAD and AND domains. BCN is a coastal area characterized by several  
21 valleys perpendicular to the coastline and two main mountain ranges, one coastal (500  
22 m height) and one pre-coastal (1000-1700 m height). These features induce mesoscale  
23 phenomena such as sea-breeze and mountain-valley winds. On the other hand, MAD is  
24 a continental region with a much simpler topography that includes the Tajo valley in the  
25 south and the mountain range of the Central System in the north, with summits reaching  
26 2500 m.

27 The urban contribution in BCN (3.1 million inhabitants) is accompanied by industrial  
28 and power generation emissions, the road network and the harbor: Meanwhile, the  
29 Spanish capital of MAD is mainly influenced by emissions from the urban area (5.8  
30 million inhabitants) and the road network that connects MAD with the surrounding  
31 commercial and industrial zones, as well as the urban areas.

1 AND is the southern-most region in Spain, with complex topography characterized by  
2 the large depression of the Guadalquivir Basin (delimited by the Iberian Massif and the  
3 Betic Range), which crosses the region from NE to SW over a 60–km stretch. About  
4 three quarters of AND has a mountainous orography, including the Sierra Nevada (3481  
5 m). AND includes one of the five biggest cities in Spain, Seville (~700 000 inhabitants),  
6 which hosts industrial and electric generation activities around the Algeciras bay, and it  
7 is affected by dense maritime traffic through the Strait of Gibraltar.

8 The study is performed for April 2013. At the beginning and end of the month, the  
9 synoptic circulation was controlled by a low pressure system located over the south of  
10 the British Isles and affected Western Europe by leading to atmospheric instability over  
11 the IP. This pattern is typical of transitional months such as April and November  
12 (García-Valero et al., 2012; Valverde et al., 2014), which produce precipitation and low  
13 temperatures because of cold and humid winds from the Atlantic Ocean. In contrast,  
14 from 12-18 April there was a high pressure system crossing the Iberian Peninsula in a  
15 SW-NE direction, transporting dust from the Sahara Desert and increased temperatures  
16 up to 25-28°C confirmed by the mineral dust forecasts of the BSC-DREAM8b model  
17 (<http://www.bsc.es/earth-sciences/mineral-dust-forecast-system/bsc-dream8b-forecast>).  
18 During the latter episode, available air quality stations in the study domains observed  
19 several exceedances of the European limit values (8 exceedances of the NO<sub>2</sub> hourly  
20 limit value, 25 exceedances of the O<sub>3</sub> information threshold, and 31 exceedances of the  
21 PM<sub>10</sub> daily limit value).

## 22 **2.2 CALIOPE-AQFS**

23 CALIOPE-AQFS has provided 48-h air quality forecasts for Europe and Spain since  
24 October 2006 ([www.bsc.es/caliope](http://www.bsc.es/caliope)) and has been described and evaluated in detail  
25 elsewhere (Baldasano et al., 2008, 2011; Pay et al., 2011, 2012a). Briefly, it integrates a  
26 meteorological model (WRF-ARW v3.5; Skamarock and Klemp, 2008), an emission  
27 model (HERMESv2; Guevara et al., 2013), a chemical transport model (CMAQv5.0.1;  
28 Byun and Schere, 2006; Appel et al., 2013), and a mineral dust atmospheric model  
29 (BSC-DREAM8bv2; Pérez et al., 2006; Basart et al., 2012); together, all of these  
30 comprise an air quality forecast system.

31 **Figure 1** shows the working domains of the CALIOPE-AQFS. First, CALIOPE-AQFS  
32 was run over Europe at 12-km x 12-km horizontal resolution using initial/boundary

1 conditions from the Final Analyses of the National Centers of Environmental Prediction  
2 (FNL/NCEP). The analyses began at 12 UTC, at intervals of 6 h (0.5°x0.5°) for  
3 meteorology. The global model LMDz-INCA2 (3.75°x2.5°, [Szopa et al., 2009](#)) was used  
4 for chemistry. Then, CALIOPE-AQFS was run at 4-km x 4-km horizontal resolution  
5 (IP4) over the IP using one-way nesting. In the present work CALIOPE-AQFS runs at 1  
6 km x 1 km over the AND, BCN and MAD domains, with a nesting of over IP4 domain.  
7 HERMESv2.0 forecasts anthropogenic emissions for the year 2009 by following a  
8 bottom-up methodology (point, linear and area), and biogenic emissions using the  
9 MEGANv2.0.4 model ([Guenther et al., 2006](#)). Emissions are aggregated into 1-km grids  
10 for AND, BCN and MAD 1-km simulations, and into 4 km grid for IP4.

11 Vertically, WRF-ARW is configured with 38 sigma layers up to 50 hPa, with 11  
12 characterizing the planetary boundary layer (PBL). Meanwhile, the CMAQ vertical  
13 levels are obtained by collapsing from the 38 WRF levels to a total of 15 layers whose  
14 depth increases with height from the surface up to 50 hPa. Six layers are within the  
15 PBL, and the first layer depth is 39 m.

16 The present WRF setup uses the Rapid Radiation Transfer Model (RRTM) and Dudhia  
17 for long- and short-wave radiation, respectively, the Kain-Fritsch cumulus  
18 parameterization ([Kain and Fritsch, 1990](#)), the single-moment 3-class (WSM3)  
19 microphysics scheme; and the Yonsei University PBL scheme (YSU). The Noah land-  
20 surface model (NoahLSM), based on the U.S. Geological Survey's (USGS) land-use  
21 data from the year 1993, is used by default in the present WRF configuration.

22 Currently, a new CMAQ version is being tested in the CMAS community, namely  
23 CMAQv5.0 ([CMAQ, 2012](#)). It includes substantial scientific improvements over  
24 Version 4.5 and is especially devoted to improving SOA formation as well as the  
25 dynamic interactions of fine and coarse aerosols. Based on the evaluation results from  
26 the previous CMAQ version within CALIOPE-AQFS (4.5 vs. 5.0) ([Pay et al. 2012b](#)),  
27 CMAQ has been updated to Version 5.0.1 using the CB05 chemical mechanism  
28 ([Yarwood et al., 2005](#)), the AERO5 for aerosol modeling, and the in-line photolysis  
29 calculation. Although not used here, future simulations will use the updated version of  
30 the aerosol module (AERO6) which includes significant improvement about the science  
31 on the primary organic aerosol aging and the sulfur chemistry.



1 CALIOPE-AQFS considers desert dust contribution by means of the BSC-  
2 DREAM8bv2, which runs off-line at a 0.5° x 0.5° resolution covering Europe, North  
3 Africa and the Middle East. Its outputs are mass conservative interpolated to the  
4 CMAQ's Lambert conformal conic grids at the required resolution and domain. After  
5 interpolating, the modeled PM<sub>10</sub> concentration is calculated as the sum of Aitken,  
6 accumulation and coarse-mode modes from CMAQ, and the corresponding BSC-  
7 DREAM8bv2 bins with a diameter of  $\leq 10 \mu\text{m}$  (Pay et al., 2012a).

### 8 **2.3 Computational strategy**

9 Running CALIOPE-AQFS at 4 and 1 km is a technical challenge. The simulations are  
10 run on MareNostrum supercomputer (Intel Xeon E5-2670, 16 CPUs and 64 GB RAM  
11 memory per node) at BSC-CNS. Table 1 depicts the computational requirements for  
12 forecasting air quality at 48 h for each domain. The number of CPUs was chosen to  
13 maximize CPU efficiency. Thanks to the parallelization of meteorological and air  
14 quality models, MareNostrum uses up to 256 CPUs. Due to the variable nature and  
15 complex dependencies, the computational time for forecasting 48 h of air quality fields  
16 for the 4 domains is 8-9 hours. The most computationally demanding domain is the  
17 AND, at 1-km resolution (366x358 cells, 256 CPU max., and 300 min). For the April  
18 2013 simulation, times add up to 2880 CPU hours/day, or 86400 CPU hours on a single  
19 processor (9.86 years). The storage for the April 2013 output files was 6.13 TB (~200  
20 GB/day).

### 21 **2.4 Evaluating the increase in resolution**

22 Comparing CALIOPE-AQFS model outputs and measurements was done for gas-phase  
23 and aerosol concentrations (O<sub>3</sub>, NO<sub>2</sub>, and PM<sub>10</sub>). Representativeness continues to be a  
24 challenge when comparing gridded simulations to observational data at a point in time  
25 and space, as modeled concentrations represent a volumetric average over an entire grid  
26 cell. Furthermore, the stochastic compound embedded in the observations is not  
27 accounted for. Concerning temporal representativeness in the present comparison, both  
28 modeled and measured concentrations are averaged hourly. CALIOPE-AQFS  
29 operationally receives air quality measurements from Spanish administrative networks  
30 in near real time (NRT) without any quality control. For the present study, NRT  
31 measurements are filtered by removing data before and after measurement interruptions



1 or calibrations. Also, a minimum cut-off threshold of  $1 \mu\text{g m}^{-3}$  is applied to the observed  
2 concentrations in order to avoid unrealistic observations. After filtering, the number of  
3 stations is 48/30/36 for  $\text{O}_3$ , 51/42/42 for  $\text{NO}_2$ , and 52/15/33 for  $\text{PM}_{10}$  in the  
4 AND/BCN/MAD domains, respectively.

5 The meteorological fields are evaluated for wind speed (U10) and wind direction  
6 (WD10) at 10 m, and temperature at 2 m (T2M). The 10 METAR stations are all  
7 located at airports (6/2/2 stations in AND/BCN/MAD) and are discussed in [Sect. S1](#).

8 [Figure 2](#) shows the location of the air quality and METAR (METeorological Aerodrome  
9 Report) stations over the respective domains. The spatial representativeness of the air  
10 quality network is highly variable. The influence of the station type is based on two  
11 classifications of air quality monitoring stations, the environment type (rural, R;  
12 suburban, S; and urban, U), and the dominant emission source (traffic, T; industrial, I;  
13 and background, B). These were derived from the Council decision 97/100/EC ([Garber  
14 et al. 2002](#)).

15 The evaluation is based on discrete statistics performed on an hourly basis. We consider  
16 the correlation coefficient ( $r$ , Eq. A1), mean (absolute, relative, and fractional) biases  
17 (MB, MNBE, and MFB, Eq. A2-A4), and error (MAE, MNGE, and MFE, Eq. A5-A7).  
18 Root Mean Square Error (RMSE, Eq. A8) is also calculated because it intensifies large  
19 differences between measured and observed concentrations (Table A1).

20 In order to evaluate the effect of increased resolution on forecast exceedances and non-  
21 exceedances of limit values established by the European legislation, we calculate  
22 categorical statistics based on comparisons with fixed concentration thresholds (T). The  
23 calculated statistics are accuracy (A, Eq. A9), bias (B, Eq. A10), probability of detection  
24 (POD, Eq. A12), critical success index (CSI, Eq. A11), and false alarm ratio (FAR, Eq.  
25 A13), whose formulas and descriptions are provided in Table A2 and also in [Kang et al.  
26 \(2005\) and Eder et al. \(2006\)](#). The 2008/50/EC directive sets an information threshold  
27 of  $180 \mu\text{g m}^{-3}$  for maximum daily  $\text{O}_3$  concentrations (Max 1h  $\text{O}_3$ ) and a target value of  
28  $120 \mu\text{g m}^{-3}$  for the maximum daily 8-h running  $\text{O}_3$  mean (Max 8h  $\text{O}_3$ ), which should not  
29 be exceeded more than 25 days per year. It establishes a limit value of  $200 \mu\text{g m}^{-3}$  for  
30 maximum daily  $\text{NO}_2$  concentrations (Max 1h  $\text{NO}_2$ ), and  $50 \mu\text{g m}^{-3}$  for the daily  $\text{PM}_{10}$   
31 mean (Mean 24h  $\text{PM}_{10}$ ), which should not be exceeded more than 35 times per year.  
32 Therefore, categorical evaluation will be performed for Max 1h  $\text{NO}_2$ , Max 1h and Max

1 8h O<sub>3</sub>, and Mean 24h PM<sub>10</sub>. Note that mean and maximum concentrations are calculated  
2 by considering at least 75% of the data in the corresponding time base, i.e., values of at  
3 least 18 hours per day for Mean 24 h, Max 1h, and Max 8h; and 6 hours for 8 h values,  
4 as established by 2008/50/EC.

### 5 **3 Concentration maps and spatial representativeness**

6 To analyze the spatial differences between resolutions, Figs. 3, 4, and 5 show the  
7 monthly mean concentration maps for April 2013 over MAD, BCN and AND domains  
8 at 4 km (left panels) and 1 km (right panels) for NO<sub>2</sub>, O<sub>3</sub>, and PM<sub>10</sub>, respectively.

9 The maps of NO<sub>2</sub> and PM<sub>10</sub> at both resolutions display similar distribution along the  
10 MAD and BCN urban plumes. On-road traffic constitutes the main source of primary  
11 pollutants in MAD and BCN. HERMESv2.0 estimates that 75% and 59% of NO<sub>x</sub>  
12 emissions are produced by on-road traffic in both domains, respectively. Consequently,  
13 when the resolution increases, the monthly mean O<sub>3</sub> concentration maps are almost  
14 identical, although the NO<sub>x</sub> titration effect on O<sub>3</sub> is significant along highways and  
15 major point sources. In AND, NO<sub>2</sub> and O<sub>3</sub> concentrations are also conserved between  
16 resolutions along the shipping route crossing the Strait of Gibraltar towards the  
17 Mediterranean Sea.

18 However, the definition of NO<sub>2</sub> concentrations along highways connecting the biggest  
19 cities with the rest of the country and industrial sectors are more easily identified at 1-  
20 km simulations than at 4 km, especially along those roads from/to Barcelona (e.g., the  
21 AP7 Mediterranean highway and C32, which connects the harbor and the airport) and  
22 Madrid (the A-2 and A-6 in the north, and A-3, A-4 and A-5 in the south). In the same  
23 way, 1-km O<sub>3</sub> maps are more textured than those at 4 km along highways, because the  
24 titration effect is more significant at 1 km, due to less dilution within grid cells. The  
25 titration effect of NO<sub>x</sub> on O<sub>3</sub> over the main sources is more forceful in BCN than in  
26 MAD, given that BCN has a larger concentration gradient resulting from complex  
27 topography and recirculation flows that accumulate pollutants.

28 The improvement of the definition along roads in AND is lower than that observed in  
29 the MAD and BCN domains, due to the fact that the AND domain is bigger and  
30 displays lower traffic emission sources than the MAD or BCN domains. Regarding  
31 PM<sub>10</sub>, the main component in AND is the desert dust (~40% in both resolutions) from  
32 North Africa. This is because there were two episodes on 14-19th and 25-26th April that

1 affected the IP, as shown by the S-N PM<sub>10</sub> gradient (Fig.5e and f). The desert dust is  
2 transported from long-range simulation with BSC-DREAM8bv2.

3 Over complex terrains, the 1-km simulation produces more realistic looking NO<sub>2</sub>  
4 concentration maps because of its more detailed topographic information. For instance,  
5 the BCN 1-km simulation displays the lowest NO<sub>2</sub> concentrations (< 10 µgm<sup>-3</sup>) along  
6 the coastal chain (500 m height) and pre-coastal chain (1000-1700 m height), except for  
7 the city's urban hill, where concentrations reach 20-40 µgm<sup>-3</sup>. In contrast, the 4-km  
8 simulation provides smoother NO<sub>2</sub> concentrations without any concentration gradient.  
9 Thus, the 1-km simulation generates slightly higher O<sub>3</sub> background concentrations than  
10 the 4-km simulation along the BCN pre-coastal chain (66-70 vs. 70-74 µgm<sup>-3</sup>), as well  
11 as across the Iberian Massif (AND), where the O<sub>3</sub> displays significant structure due to  
12 the higher resolution topography that follows the basin and the areas of high-density on-  
13 road traffic.

14 Figures 3, 4, and 5 include dots corresponding to mean concentrations at air quality  
15 stations that help to qualitatively evaluate the modeled spatial representativeness at both  
16 resolutions. Note the strong correlation between NO<sub>2</sub> observations and the 1-km  
17 simulation near the primary suburban traffic roads in BCN (e.g., Vilafranca, Igualada,  
18 Manresa, and Mataró). Regarding O<sub>3</sub>, although observed concentrations depict an  
19 overall tendency of the model to underestimate concentrations at both resolutions, the 1-  
20 km simulation shows better agreement with measurements at rural background stations  
21 (e.g., El Atazar, San Martín, Villa de Prado, Villarejo and Orosco stations in MAD), and  
22 at suburban traffic stations (e.g., Manresa, Igualada and Vilafranca in BCN, with  
23 modeled O<sub>3</sub> concentrations of around 54-58 µgm<sup>-3</sup> at 1 km, and 60-66 µgm<sup>-3</sup> at 4 km).  
24 For PM<sub>10</sub>, comparisons with measurements show that modeled concentrations are  
25 underestimated over background areas, mainly outside the urban/suburban areas, as  
26 already discussed in Pay et al. (2012a). However, PM<sub>10</sub> measurements at the  
27 urban/suburban stations of Vilafranca, Sant Celoni, and Mataró in BCN (14-16 µgm<sup>-3</sup>)  
28 show a higher correlation at 1 km than at 4 km (12-14 µgm<sup>-3</sup> vs. 8-10 µgm<sup>-3</sup>).

29 The spatial variability of the increased resolution is quantitatively analyzed by means of  
30 concentration maps, shown in Fig. 6 for NO<sub>2</sub>, O<sub>3</sub> and PM<sub>10</sub> over AND, BCN and MAD.  
31 Over all domains, the correlation improves as a function of the resolution increase for  
32 NO<sub>2</sub> and O<sub>3</sub>, indicated by the increase in monthly r from 0.79 (4 km) to 0.81 (1 km) for

1 NO<sub>2</sub>, and from 0.69 to 0.73 for O<sub>3</sub>. The slopes improve with the resolution increase,  
2 from 0.72 (4 km) to 0.77 (1 km) for NO<sub>2</sub>, and from 0.50 (4 km) to 0.54 (1 km) for O<sub>3</sub>.  
3 This results from the improved model performance at urban stations, indicating that  
4 CALIOPE-AQFS better captures the magnitude of the variability between urban regions  
5 at 1 km than at 4 km. In contrast, for PM<sub>10</sub>, the monthly r decreases from 0.67 to 0.58  
6 when the resolution increases. While the PM<sub>10</sub> spatial variability over BCN and MAD  
7 improves when the resolution increases (r increases by 0.01 and 0.04, respectively), the  
8 global correlation coefficient decreases at the AND stations (52/100) by 0.1 from 0.36  
9 (4 km) to 0.26 (1 km). Despite the unfavorable effect of the resolution increase in PM<sub>10</sub>  
10 over AND, the NO<sub>2</sub> and O<sub>3</sub> concentrations show the highest absolute increase for the  
11 spatial r over this domain, from 0.62 (4 km) to 0.71 (1 km) for NO<sub>2</sub> and from 0.58 (4  
12 km) to 0.64 (1 km) for O<sub>3</sub> (increasing r by 0.09 and 0.06, respectively).

## 13 **4 Temporal evaluation**

### 14 **4.1 Pollutant**

15 [Table 2](#) presents the statistical evaluation by pollutant, with a focus on the reproduction  
16 of high concentrations established by the European directive (2008/50/EC). Depending  
17 on the pollutant's lifetime and variability, as well as its dependency on precursors,  
18 increased resolution shows different impacts. The resolution increase has a positive  
19 effect on NO<sub>2</sub>, decreasing its bias by 2.0 μgm<sup>-3</sup> (from -4.5 to -2.5 μgm<sup>-3</sup>) but it also  
20 increases the absolute (squared) error by 0.3 μgm<sup>-3</sup> to 0.9 μgm<sup>-3</sup>. This positive effect is  
21 sustained by the relative variability, where the MB (MFB) is reduced by 42% (19%) and  
22 MAE (MFE) only increases by 2% (1%). The r does not between resolution (r=0.54)  
23 partially due to the fact that the NO<sub>2</sub> is a primary pollutant and emissions at both  
24 resolutions are modeled using the same approach. The bias improvement at 1-km  
25 resolution is justified, because in theory the higher resolution leads to better emission  
26 allocation from point, linear or area sources, decreases the artificial dilution of  
27 emissions compared to the larger grid area and, due to the decrease of artificial dilution,  
28 it treats chemistry more properly near large emission sources.

29 In contrast, the resolution increase has a negative effect on hourly and Max 8h O<sub>3</sub>  
30 concentrations increasing the bias and error by 0.1-0.8 μgm<sup>-3</sup>. Relative (fractional) bias  
31 and error increase by 8% (15%) and 1% (1%), respectively, for hourly O<sub>3</sub>; and 6% and  
32 4% for Max 1h O<sub>3</sub>.

1 According to the categorical evaluation, only a few exceedances of the European target  
2 and limit values were detected for Max 1h NO<sub>2</sub> (9), Max 1h O<sub>3</sub> (25), and Mean 24h PM<sub>10</sub>  
3 (31) in April 2013. Thus, categorical evaluation is performed on the temporal basis  
4 established by the European legislation, but it uses a T based on the 75<sup>th</sup> percentile (75p)  
5 of the observed concentrations in each case, where T is 71 μgm<sup>-3</sup> for Max 1h NO<sub>2</sub>, 108  
6 (101) μgm<sup>-3</sup> for Max 1h (Max 8h) O<sub>3</sub>, and 27 μgm<sup>-3</sup> for Mean 24h PM<sub>10</sub>.

7 Overall, CALIOPE-AQFS underestimates exceedances at both resolutions, indicating  
8 that errors of missing observed exceedances are not completely resolved by an  
9 increasing the horizontal resolution (a<d). The best performance is found for Max 1h  
10 NO<sub>2</sub>, where categorical bias (B, Eq. A10) improves from 37% (4 km) to 40% (1 km),  
11 although the tendency to underestimating exceedances remain with the resolution  
12 increase (B < 100%).

13 For NO<sub>2</sub> Max 1h, there are 953 observed exceedances (b+d) of the threshold (T=47  
14 μgm<sup>-3</sup>). Increasing the resolution increases the POD from 49% (4 km) to 56% (1 km).  
15 As with POD, CSI examines the exceedances, but in a more comprehensive way by  
16 considering both false alarms and missing events. POD and CSI increase by 14% and  
17 20%, respectively, when resolution is increased form 4 km to 1 km. For O<sub>3</sub>, POD has a  
18 relatively low POD value, and it decreases as the resolution increases. Of the 1306  
19 observed exceedances of the 108 μgm<sup>-3</sup> Max 1h, CALIOPE-AQFS detected 112  
20 exceedances at 4 km and only 96 at 1 km. Increasing resolution decreases POD and CSI  
21 by 22% and 25% for O<sub>3</sub> Max 1h, whereas they do not significantly change for Max 8h  
22 O<sub>3</sub> and Mean 24h PM<sub>10</sub>.

23 FAR increases for Max 1h NO<sub>2</sub> (from 40% to 42%) and decreases for Max 1h O<sub>3</sub> (from  
24 27% to 17%) when the resolution increases. In relative terms, this variability is more  
25 significant for Max 1h O<sub>3</sub> (37 %) than for Max 1h NO<sub>2</sub> (5%), indicating that, in terms of  
26 failures, the resolution has a positive global effect by reducing false exceedances.

27 For various reasons, accuracy (A) remains almost constant when the resolution  
28 increases. For NO<sub>2</sub> and O<sub>3</sub>, this is due to a stable sum of b and c, increasing the b at the  
29 cost of c, and vice versa. For NO<sub>2</sub>, the number of hits (b) to forecast Max 1h at 1 km is  
30 higher than 4 km (537 vs. 466), but the number of correct negatives at 1 km is lower  
31 than at 4 km (2439 vs. 2517). The resolution increase has the opposite effect on O<sub>3</sub>,

1 decreasing the number of hits by 14% for Max 1h and 33% for Max 8h. The increase of  
2 the number of correct negatives is less than 2% in both Max 1h and Max 8h O<sub>3</sub>.

### 3 **4.2 PM<sub>10</sub> components**

4 The resolution increase has the lowest effect on PM<sub>10</sub> hourly concentrations and its  
5 exceedances (<1%). PM<sub>10</sub> components are secondary inorganic aerosols (SIA), which  
6 include sulfate (SO<sub>4</sub> = SO<sub>4</sub><sup>2-</sup>), nitrate (NO<sub>3</sub> = NO<sub>3</sub><sup>-</sup>), ammonium (NH<sub>4</sub> = NH<sub>4</sub><sup>+</sup>),  
7 secondary organic aerosol (SOA), elemental carbon (EC), sea salt (SS), desert dust  
8 (DD), and primary PM (PPM).

9 [Pay et al. \(2012a\)](#) evaluated the PM components at some urban and rural background  
10 stations in Spain using the CALIOPE-AQFS based on CMAQv4.5, where they showed  
11 that the model underestimated SIA by a factor of 2-3. The highest underestimation was  
12 found for fine carbonaceous aerosols (a factor of 4), in part related to the state-of-the-  
13 science concerning SOA formation pathways. The updated version of CMAQ, v5.0.1  
14 includes scientific improvements to SOA formation and aerosol dynamics, which could  
15 improve the modeled PM<sub>10</sub> performance and its components.

16 [Figure 8a](#) shows that the resolution increase does not significantly change the PM<sub>10</sub>  
17 composition. DD remains the main contributor (~40-41%), followed by PPM (22-24%),  
18 SIA (~21-22%), SS (9-11%), EC (~4%) and SOA (~0.6%). However, the effect of the  
19 increased resolution on PM<sub>10</sub> component concentrations is different ([Fig. 8b](#)),  
20 depending on their origin, atmospheric cycle and the way they are modeled. DD  
21 concentrations do not change between resolutions, because they are mass conservative  
22 when interpolated from 0.5°x0.5° till 1 km x 1 km.

23 For SIA, increasing the resolution increases NO<sub>3</sub> and NH<sub>4</sub> concentrations by 4 and  
24 ~2%, respectively, and it decreases SO<sub>4</sub> by ~2%. The NH<sub>4</sub> increase means there are  
25 more primary precursors (H<sub>2</sub>SO<sub>4</sub> or HNO<sub>3</sub>/NO<sub>2</sub>) available to neutralize NH<sub>3</sub> (gas) to  
26 NH<sub>4</sub> (aerosol). However, the variability between SO<sub>4</sub> and NO<sub>3</sub> is more difficult to  
27 explain, due to the nonlinearity of photochemistry and aerosol formation, which is  
28 controlled to some extent by the ISORROPIA thermodynamic equilibrium.  
29 Furthermore, the absence of aerosol measurements for April 2013 does not allow us to  
30 investigate this further.

1 The resolution increase results in a decrease in SS of ~16%, the largest change of all the  
2 PM<sub>10</sub> components. CMAQv5.0.1 simulates SS emission as a function of the wind speed  
3 and the relative humidity (Gong, 2003; Zhang et al., 2005). Although not shown here,  
4 when the resolution increases, the wind speed decreases at the available PM<sub>10</sub> stations  
5 by ~1.4/0.4/0.2 ms<sup>-1</sup> over AND/BCN/ MAD, and also over the open ocean.

6 For primary PM components EC and PPM, increasing resolution results in higher  
7 concentrations (by 10 and ~12%, respectively). As for NO<sub>2</sub>, the 1-km simulation leads  
8 to a reduced effect of artificial dilution of emissions in a grid cell, so concentration  
9 gradients are stronger than in the 4-km simulation.

### 10 **4.3 Domain**

11 The resolution increase has varying impacts due to differences in geographical location  
12 and emission patterns over the domains (Fig. 7). BCN shows the highest NO<sub>2</sub> bias  
13 decrease (73%) when the resolution increases, but no effect on the correlation (<7%).  
14 However, O<sub>3</sub> shows significant variability over BCN, increasing r by 4% and MB by  
15 23%. To a lesser extent, MB also increases over AND (by 8%). Meanwhile, the  
16 variability over MAD is reduced (bias differences <4%). MB decreases for PM<sub>10</sub> (bias  
17 differences <1 μgm<sup>-3</sup>) over the urban domains of MAD (3%) and BCN (16%), and  
18 increases over AND (7%).

19 Figure 9 analyzes the impact of the resolution increase on daily cycles. Although PBL  
20 measurements are not available, PBL daily cycles are displayed together in order to find  
21 some correlations with the daily pollutant variability. Due to the lamination of PBL  
22 growth by the Mediterranean sea breezes, the PBL reaches its maximum height at  
23 midday, being the highest in MAD (1600 m AGL) followed by AND (1000 m AGL)  
24 and BCN (900 m AGL).

25 As shown in Sect. S1, the pollutant transport at the BCN coastal domain is controlled by  
26 mesoscale phenomena such as sea-breezes (day) and land-breezes (night), which are a  
27 result of its complex topography and location (Baldasano et al., 1994; Millán et al.,  
28 1997; Gonçalves et al., 2009). The NO<sub>2</sub> daily cycle is highly influenced by traffic  
29 emissions (Fig. 9). Both resolutions show the highest underestimations for the morning  
30 peak (6 am) (~20 μgm<sup>-3</sup>). Although the afternoon peak is well reproduced, there is  
31 excessive variability at both resolutions, a result of problems with wind direction.



1 During the sea breeze period, the mean simulated wind was more easterly than westerly,  
2 as registered by measurements (Sect. S1). Several works indicate that WRF has  
3 difficulty reproducing the morning and evening transition over the urban environment,  
4 possibly because it does not model the heat retention in cities (Makar et al., 2006; Appel  
5 et al., 2013). Increasing the resolution increases NO<sub>2</sub> concentrations by 21% from 14  
6 μgm<sup>-3</sup> (4 km) to 17 μgm<sup>-3</sup> (1 km) during the morning hours after sunrise (5-9 am) and in  
7 the evening hours after sunset (5-9 pm). This behavior could be explained by PBL  
8 variability when increasing the resolution, which decreases PBL height by ~33 m for  
9 these hours.

10 NO<sub>2</sub> performance impacts the O<sub>3</sub> daily cycles over BCN, showing that 4- and 1-km  
11 simulations underestimate maximum O<sub>3</sub> concentrations by ~20 μgm<sup>-3</sup> at midday (1-4  
12 pm) and overestimate minimum O<sub>3</sub> concentrations by ~20 μgm<sup>-3</sup> in the morning hours  
13 after sunrise (5-9 am). The resolution increase results in slightly lower O<sub>3</sub>  
14 concentrations at night, which is perhaps the result of lower PBL heights in the 1-km  
15 simulation during the early morning and late afternoon, when PBL height tends to be  
16 the lowest. During these hours, the titration effect of NO<sub>2</sub> on O<sub>3</sub> is greater, improving  
17 the O<sub>3</sub> overestimation of the daily minimum, which allows a slightly higher hourly r  
18 (2%). However, O<sub>3</sub> underestimation increases in the late afternoon, contributing to an  
19 increase in the hourly mean bias from ~9 μgm<sup>-3</sup> (4 km) to ~11 μgm<sup>-3</sup> (1 km).

20 In BCN, the PM<sub>10</sub> underestimation is not systematic throughout the daily cycle (Fig. 9),  
21 which shows a bias of ~20 (10) μgm<sup>-3</sup> at day (night) time. The higher daytime  
22 underestimation as compared to the nighttime cannot be explained by the current  
23 results, but it could be a result of missing sources (e.g., fugitive agricultural emissions  
24 and wind-blown dust) and problems with PBL height overestimation and an excess  
25 dilution of emissions. The resolution increase reduces the bias by ~1 μgm<sup>-3</sup> (16%),  
26 especially during early morning and late afternoon, when the highest PBL height  
27 variability between resolutions is observed. Although the evaluation of T2M, U10 and  
28 WD10 indicates that the resolution increase has a small effect over BCN (Sect. S1), the  
29 reduction of the artificial dilution of NO<sub>2</sub> emissions –together with a lower PBL height  
30 at 1 km than at 4 km during the night and early morning– improves NO<sub>2</sub>, O<sub>3</sub> and PM<sub>10</sub>  
31 concentrations, which in turn decreases their biases.

1 For AND, the model underestimates observed NO<sub>2</sub> concentrations throughout the daily  
2 cycle by ~5 μgm<sup>-3</sup> for both the 4-km and 1-km simulations, with the highest  
3 underestimation during the morning peak (~25 μgm<sup>-3</sup>) and the lowest during the  
4 afternoon peak (~10 μgm<sup>-3</sup>). The resolution increase reduces the bias from -3.5 to -2  
5 μgm<sup>-3</sup> (by 43%) and increases r by 7% (from 0.39 to 0.41). As in BCN, the NO<sub>2</sub>  
6 underestimation directly impacts the O<sub>3</sub> daily cycle (which the resolution increase  
7 cannot resolve), increasing the bias by ~1 μgm<sup>-3</sup>, a phenomenon that is predominant in  
8 the morning hours. In the case of PM<sub>10</sub>, the daily cycle indicates that the biases are  
9 almost systematic throughout the day (~22 μgm<sup>-3</sup>). Increasing the resolution increases  
10 the bias by less than 4% in the late afternoon, which is perhaps dominated by the  
11 decrease in PBL height. When the resolution is increased, NO<sub>2</sub> performs better partially  
12 due to the improved model performance for the temperature and wind speed (Sect. S1),  
13 as well as the lower nighttime and higher daytime PBL. Meanwhile, the O<sub>3</sub> and PM<sub>10</sub>  
14 performance do not significantly change.

15 During April 2013, the main flow over MAD was controlled by S-SW synoptic winds  
16 channeled by orographic barriers in the NW domain and the Tajo valley (Valverde et  
17 al., 2014). The NO<sub>2</sub> daily cycle depicts a high influence of traffic emissions (Fig. 9),  
18 showing significant model underestimation at both resolutions for the  
19 morning/afternoon peaks (~15/10 μgm<sup>-3</sup>). Note that, in terms of temporal variability of  
20 the NO<sub>2</sub> concentrations, the model performs well at the afternoon peak when the air  
21 flow is controlled by southeastern winds. The NO<sub>2</sub> performance leads to more accurate  
22 O<sub>3</sub> daily cycles than in AND and BCN, especially in the early morning, when the  
23 titration effect of NO<sub>2</sub> is greater because the NO<sub>2</sub> morning peak underestimation is  
24 smaller when compared to the other domains. Meanwhile, the modeled PM<sub>10</sub> at both  
25 resolutions presents a profile controlled by traffic emissions. Observed concentrations  
26 display a flatter daily cycle, in which the model underestimation reaches 40 μgm<sup>-3</sup> in the  
27 morning. Increasing resolution shows a positive effect for NO<sub>2</sub> and PM<sub>10</sub> because it  
28 increases r by 0.01 and reduces MB and RMSE by 0.1-0.2 μgm<sup>-3</sup>. However, it has the  
29 lowest variability when compared to the other domains (<5 % for bias, error and r),  
30 likely the result of a relatively simpler topography and meteorological patterns.

#### 1 **4.4 Environment and major sources**

2 [Figure 7](#) shows that the resolution impact also depends on the type of area and the  
3 dominant emission source. Theoretically, the meteorological fields of urban areas differ  
4 from those of surrounding rural areas because of their different morphology (radiation  
5 trapping and wind profiles), surface materials (heat storage) and variable energy  
6 consumption (heat release).

7 Increasing resolution reduces the NO<sub>2</sub> bias at suburban and urban stations by 1.8-2 μgm<sup>-3</sup>  
8 <sup>3</sup>, and to a lesser extent by 1.2 μgm<sup>-3</sup> at rural stations. The correlation coefficients also  
9 improve at suburban stations (from 0.48 to 0.52) and rural stations (from 0.34 to 0.35).  
10 This may be due to better allocation of land-use categories (urban vs. rural) and of their  
11 fraction in a grid cell in the 1-km simulation than in 4-km simulation. The NO<sub>2</sub> bias  
12 decreases by 39% (65%) at urban (background) stations, but O<sub>3</sub> biases increase by 9%  
13 (5%). For PM<sub>10</sub>, the resolution increase does not significantly change as a function of  
14 area type, with differences in bias and error of less than ±4% (<0.5 μgm<sup>-3</sup>) between the  
15 two resolutions.

16 The low improvement at urban stations may be because the NoahLSM land-surface  
17 model does not consider the effect of urban morphology or thermal parameters in order  
18 to accurately model meteorological fields. Modeling air quality on an urban scale over  
19 cities requires a description of the heat/momentum exchange between buildings and the  
20 lower atmospheric layers. For instance, the impact of using an urban model on  
21 meteorological fields over the greater Paris area was studied by [Kim et al. \(2013\)](#) using  
22 WRF with the Urban Canopy Model, demonstrating that below 1 km height  
23 overestimations of wind speed were significantly reduced.

24 The impact on r of increasing resolution is less than 2% for primary pollutants near  
25 important emission sources. For example, it reduces NO<sub>2</sub> biases at traffic (industrial)  
26 stations by ~3 μgm<sup>-3</sup> (2 μgm<sup>-3</sup>), but it increases O<sub>3</sub> biases by ~2 μgm<sup>-3</sup> (1 μgm<sup>-3</sup>).  
27 However, the resolution increase in the range of 4-1 km does not exhibit the expected  
28 improvement on the hourly statistics that are based on the constraints of the current  
29 model formulation. In other words, it cannot resolve the subgrid air quality variability  
30 merely by increasing resolution. For instance, although on-road traffic emissions are  
31 estimated by following a bottom-up approach along highways and routes, heterogeneity  
32 is lost in the CTM volume averaging process, which artificially dilutes emission rates

1 over the grid cells. The resolution effect is low at background stations, which generally  
2 are not influenced by any single source, but rather by the integrated contribution from  
3 all sources upwind of the stations where variations are less than 1% for O<sub>3</sub> and PM<sub>10</sub> (<  
4 1 μgm<sup>-3</sup>). However, background NO<sub>2</sub> levels increase by ~1 μgm<sup>-3</sup> (48%) from 4 km to 1  
5 km.

6 [Figure 10](#) shows the temporal series and daily cycles for NO<sub>2</sub> and O<sub>3</sub> at traffic and  
7 background stations throughout the episode of 12-18<sup>th</sup> April, 2013. At traffic stations,  
8 the temporal series show a remarkable O<sub>3</sub> daily cycle (observed 25p = 23.2 μgm<sup>-3</sup> and  
9 75p = 77.5 μgm<sup>-3</sup>), due to O<sub>3</sub> destruction caused by high NO<sub>x</sub> levels (observed 50p =  
10 34.5 μgm<sup>-3</sup>). In contrast, the NO<sub>2</sub>-limited regime at background sites (observed 50p =  
11 19 μgm<sup>-3</sup>) allows for higher O<sub>3</sub> concentrations (observed 25p = 38 μgm<sup>-3</sup> and 75p = 89  
12 μgm<sup>-3</sup>) than in high NO<sub>2</sub> environments.

13 During the episode mentioned above, the resolution increase at traffic stations had a  
14 positive effect by increasing the r for NO<sub>2</sub> (from 0.73 to 0.76) and O<sub>3</sub> (from 0.83 to  
15 0.86), and also decreasing the NO<sub>2</sub> mean bias by ~5 μgm<sup>-3</sup> (from 6 to 1 μgm<sup>-3</sup>). The  
16 NO<sub>2</sub> daily cycle improves in the morning hours after sunrise, reducing bias by 5-10  
17 μgm<sup>-3</sup> and contributing to a reduction in O<sub>3</sub> overestimations (~5 μgm<sup>-3</sup>). In contrast, at  
18 background stations, where the NO<sub>x</sub>/O<sub>3</sub> chemistry is less dominant, the resolution effect  
19 is not significant. Such behavior indicates that finer resolution improves the model  
20 performance, because horizontal resolution affects the representation of chemical  
21 processes near large emission sources, such as the formation of O<sub>3</sub> and nighttime O<sub>3</sub>  
22 titration ([Mathur et al., 2005](#)).

## 23 **5 Conclusions**

24 The present work shows the effects of increasing the horizontal resolution from 4 km to  
25 1 km using the CALIOPE-AQFS on pollutant concentrations (NO<sub>2</sub>, O<sub>3</sub>, and PM<sub>10</sub>) over  
26 three Spanish domains (AND, BCN and MAD) in April 2013.

27 The global features of concentration maps at both resolutions are quite similar, with  
28 zones of high/low concentration identically located, which is expected since both  
29 simulations are based on the same emission dataset. Further comparisons demonstrate  
30 that increasing the resolution provides better-defined and more realistic concentration  
31 structures over large emission sources (roads and industries) and complex terrains (more  
32 sharply defined orographic hills). The titration effect on O<sub>3</sub> by NO<sub>x</sub> along highways and

1 major point sources is more evident in 1-km simulations than at 4 km, since NO<sub>x</sub>  
2 concentrations tend to be higher in the 1-km simulation due to less dilution. This  
3 improvement is quantified by an increase in spatial correlation coefficients of 3% (6%)  
4 for NO<sub>2</sub> (O<sub>3</sub>).

5 However, the resolution increase in the range of 4-1 km does not exhibit the expected  
6 improvement in hourly statistics for any pollutant. Hourly correlation coefficients do  
7 not significantly change, and absolute (relative) errors and biases vary < 2 μgm<sup>-3</sup> (9%).  
8 The merit of the resolution increase may be underrated when classical statistics are  
9 applied at measurement stations (Mass et al., 2002; Gego et al., 2005). For instance,  
10 although the structure of important NO<sub>2</sub> urban plume features (> 40 μgm<sup>-3</sup>) often  
11 become more realistic (stronger and more defined plumes) as resolution increases,  
12 statistics are deeply degraded by even small timing and spatial errors.

13 The resolution increase has a significant impact on reducing NO<sub>2</sub> hourly bias (by 42%,  
14 2 μgm<sup>-3</sup>), without any significant change in the error and the r (<2%). However, O<sub>3</sub>  
15 hourly biases increased by <1 μgm<sup>-3</sup>. The main differences between resolutions appear  
16 at daytime and nighttime traffic peaks, when the mixing height experiences rapid  
17 changes, allowing the 1-km simulation to slightly reduce NO<sub>2</sub> underestimation in the  
18 morning by ~5-10 μgm<sup>-3</sup>. The O<sub>3</sub> daily cycles at large emission sources depict a high  
19 influence of hourly NO<sub>2</sub> concentrations, increasing the hourly O<sub>3</sub> bias by ~3 μgm<sup>-3</sup>. This  
20 behavior is controlled by the daytime O<sub>3</sub> underestimation and, to a lesser extent, by the  
21 nighttime overestimation. The resolution increase reduces the O<sub>3</sub> overestimations at  
22 night by ~5 μgm<sup>-3</sup> partly because of higher nocturnal NO<sub>2</sub> concentrations.

23 Increasing the horizontal resolution improves the model's ability to forecast 75p  
24 exceedances in the observed maximum 1h concentrations. The number of hits that  
25 forecast 75p exceedances in the observed Max 1h NO<sub>2</sub> increases from 466 to 537 over  
26 953 exceedances, while the FAR for Max 1h O<sub>3</sub> exceedances is reduced by 37%.

27 The grid effect is less pronounced for PM<sub>10</sub> than for NO<sub>2</sub> and O<sub>3</sub>. When the resolution  
28 increases, the low gradient of PM<sub>10</sub> mean concentrations (<0.1 μgm<sup>-3</sup>) is the result of  
29 compensating biases of PM<sub>10</sub> components, which is controlled mainly by the PPM and  
30 EC increase, as well as the SS decrease.

1 BCN is the domain where the resolution increase has the largest effect, with changes in  
2 bias (error) of 16-73% (< 5%), followed by AND with 4-43% (< 5%) and MAD < 3-5%  
3 (< 1%). In BCN, as in the western Mediterranean Basin, the transport of O<sub>3</sub> and its  
4 precursors is governed by mesoscale circulations. In that sense, the resolution increase  
5 has a large impact over BCN, where induced mesoscale phenomena control the air flow.  
6 Conversely, synoptic transport is more prominent in MAD and AND. Increasing the  
7 resolution to 1 km over rural areas ([Mass et al., 2002](#)) could contribute to improve the  
8 representation of mesoscale meteorological structures such as orographic wind and  
9 circulation. Over urban areas along the western Mediterranean coast, further  
10 improvements (e.g., models that consider the urban morphology and thermal  
11 parameters) are required before seeing any benefits in increasing the resolution to 1 km  
12 ([Toll and Baldasano, 2002](#); [Jiménez et al., 2006](#); [Fay and Neunhäuserer, 2006](#)).

13 In urban areas and near large emission sources (industrial and traffic stations), NO<sub>2</sub> and  
14 O<sub>3</sub> concentrations are more sensitive to changes in the grid resolution. The  
15 concentration increases in primary anthropogenic pollutants (NO<sub>2</sub>, PPM and EC)  
16 because the high resolution may better allocate emissions at point, linear and area  
17 sources. Increase resolution also reduces the artificial dilution of emissions when  
18 compared to the larger grid area. Despite the reasons above, moving to 1-km horizontal  
19 resolution generally did not result in better performance for O<sub>3</sub> and NO<sub>2</sub>.

20 This analysis demonstrates weaknesses in the current model formulations that cannot be  
21 resolved with only high-resolution modeling. The subgrid air quality variability at 1-km  
22 resolution could be not reproduced over large emission sources or urban areas, because  
23 a finer spatial structure is expected but unresolved. While the work presented here  
24 demonstrates the feasibility of modeling at fine-scales, there remain many challenges.  
25 First, there is a loss of subgrid emission heterogeneity. Emission inputs to CTM are an  
26 average rate, which accounts for the volume averaged quantity of mass released per unit  
27 of time. No other information regarding emission allocation (e.g., point, linear or per  
28 area) is considered; for instance a large amount of mass can be emitted by a small  
29 portion of the grid surface or by several sources scattered around it ([Galmarini et al.,  
30 2008](#); [Cassiani et al., 2010](#); [Ching and Majeed, 2012](#)). Despite the fact that emissions  
31 are estimated by following a bottom-up approach emission model, emission  
32 heterogeneity is lost in the volume averaging process performed within CTM. The loss  
33 is even higher when resolution decreases (from 1 km to 4 km). Second, there is a low

1 degree of complexity in flow and dispersion details at urban scales, where most of the  
2 pollutants come from street canyons and/or tree canopies, where they are transported  
3 until mixing conditions allow the pollutants to disperse above these urban canopy levels  
4 ([Kim et al., 2013](#); [Ching, 2013](#)). Third, the USGS land-use data used in the WRF model  
5 is based on 1993 data, and urban changes in MAD and BCN over the last 20 years are  
6 significant.

7 Since temperature and wind speed are very sensitive to the ratio of building width to  
8 road width, future improvement for fine-scale modeling should focus on using an urban  
9 canopy model that considers effects on the transfer of energy and momentum between  
10 urban structures and the lower atmosphere. This is crucial for modeling meteorology  
11 and air quality at fine-scales in urban environments. However, it requires an urban  
12 canopy scheme and a canopy parameter database (urban fraction, building height and  
13 area). Furthermore, in order to gain any benefits from increasing resolution, the  
14 meteorological modeling should be updated to include a better description of land use,  
15 instead of relying on USGS data from the year 1993. To this end, the Coordination of  
16 Information on the Environment (CORINE) provides a high resolution (100 m) land use  
17 database, which was developed by the European Environmental Agency and updated to  
18 the year 2006 (CLC2006) (EEA, 2007). This could be implemented in the WRF model  
19 following the methodology described in [Pineda et al. \(2004\)](#).

20  
21  
22  
23  
24  
25  
26  
27  
28



1

2

3 **Appendix A**

4 Table A1. Definition of the discrete statistics used in the evaluation. Where  $C_m(x, t)$  and  
 5  $C_o(x, t)$  are the modeled and observed concentrations at a location (x) and time (t); N is  
 6 the number of pairs of data.  $\bar{C}_m$  and  $\bar{C}_o$  are the modeled and observed mean  
 7 concentrations over the whole period, respectively.

Statistic	Formula	
Correlation coefficient	$r = \frac{\sum_{i=1}^N (C_m(x, t) - \bar{C}_m)(C_o(x, t) - \bar{C}_o)}{\sqrt{\sum_{i=1}^N (C_m(x, t) - \bar{C}_m)^2} \sqrt{\sum_{i=1}^N (C_o(x, t) - \bar{C}_o)^2}}$	A1
Mean bias	$MB = \frac{1}{N} \sum_{i=1}^N (C_m(x, t) - C_o(x, t))$	A2
Mean normalized bias error	$MNBE = \frac{1}{N} \sum_{i=1}^N \frac{(C_m(x, t) - C_o(x, t))}{C_o(x, t)} \cdot 100$	A3
Mean fractional bias	$MFB = \frac{1}{N} \sum_{i=1}^N \frac{(C_m(x, t) - C_o(x, t))}{(C_o(x, t) + C_m(x, t)) / 2} \cdot 100$	A4
Mean absolute error	$MAE = \frac{1}{N} \sum_{i=1}^N  C_m(x, t) - C_o(x, t) $	A5
Mean normalized gross error	$MNGE = \frac{1}{N} \sum_{i=1}^N \frac{ C_m(x, t) - C_o(x, t) }{C_o(x, t)} \cdot 100$	A6
Mean fractional error	$MFE = \frac{1}{N} \sum_{i=1}^N \frac{ C_m(x, t) - C_o(x, t) }{(C_m(x, t) + C_o(x, t)) / 2} \cdot 100$	A7
Root mean squared error	$RMSE = \sqrt{\frac{1}{N} \sum_{i=1}^N (C_m(x, t) - C_o(x, t))^2}$	A8

8

9 Table A2. Definition of the categorical statistics used in the evaluation. Exceedance  
 10 analysis is based on a comparison with a fixed threshold concentration (T), where a is  
 11 the number of false alarms, b is the number of hits, c is the number of correct negatives,  
 12 and d is the number of misses.

Statistic	Formula
-----------	---------

---

Accuracy	$A = \left( \frac{b+c}{a+b+c+d} \right) \cdot 100$	A9
Bias	$B = \left( \frac{a+b}{b+d} \right) \cdot 100$	A10
Critical success index	$CSI = \left( \frac{b}{a+b+d} \right) \cdot 100$	A11
Probability of detection	$POD = \left( \frac{b}{b+d} \right) \cdot 100$	A12
False alarm ratio	$FAR = \left( \frac{a}{a+b} \right) \cdot 100$	A13

---

1

## 2 **Acknowledgements**

3 The Spanish administrations “Generalitat de Catalunya”, “Junta de Andalucía”, and  
4 “Comunidad de Madrid” are acknowledged for providing air quality measurements. The  
5 CALIOPE-AQFS team (G.Arévalo, K. Serradell, D. Carrió, M. Castrillo, A. Soret, S.  
6 Basart and S. Gassó) and F. Benincasa are also thanked for their technical support. This  
7 work is funded by the post-doctoral grant held by M.T. Pay in the Beatriu de Pinós  
8 programme (2011 BP-A 00427), Andalusian contract (NET838690), and the Severo  
9 Ochoa Program awarded by the Spanish Government (SEV-2011-00067).

## 1 **References**

- 2 Appel, K.W., Pouliot, G.A., Simon, H., Sarwar, G., Pye, H.O.T., Napelenok, S.L.,  
3 Akhtar, F., and Roselle, S.J.: Evaluation of dust and trace metal estimates from the  
4 Community Multiscale Air Quality (CMAQ) model version 5.0, *Geosci. Model Dev.*, 6,  
5 883-899, doi:10.5194/gmd-6-883-2013, 2013.
- 6 Baldasano, J. M., Cremades, L., and Soriano, C.: Circulation of Air Pollutants over the  
7 Barcelona Geographical Area in Summer, in: *Proceedings of Sixth European*  
8 *Symposium Physico-Chemical Behaviour of Atmospheric Pollutants*, Varese (Italy),  
9 18–22 October, 1993, Report EUR 15609/1 EN, 474–479, 1994.
- 10 Baldasano J.M, Jiménez-Guerrero, P., Jorba, O., Pérez, C., López, E., Güereca, P.,  
11 Martín, F., García-Vivanco, M., Palomino, I., Querol, X., Pandolfi, M., Sanz, M.J., and  
12 Diéguez, J.J.: CALIOPE: An operational air quality forecasting system for the Iberian  
13 Peninsula, Balearic Islands and Canary Islands- First annual evaluation and ongoing  
14 developments, *Adv. Sci. Res.* 2, 89-98, 2008.
- 15 Baldasano, J.M., Pay, M.T., Jorba, O., Gassó, S., and Jiménez-Guerrero, P.: An annual  
16 assessment of air quality with the CALIOPE modeling system over Spain, *Sci. Total*  
17 *Environ.*, 409, 2163-2178, 2011.
- 18 Basart, S., Pérez, C., Nickovic, S., Cuevas, E., and Baldasano, J.M.: Development and  
19 evaluation of the BSC-DREAM8b dust regional model over Northern Africa, the  
20 Mediterranean and the Middle East, *Tellus Series B – Chemical and Physical*  
21 *Meteorology*, 64, 1-12, 2012.
- 22 Byun, D. W. and Schere, K. L.: Review of the governing equations, computational  
23 algorithms and other components of the Models-3 Community Multiscale Air Quality  
24 (CMAQ) Modeling System, *App. Mech. Rev.* 59, 51-77, 2006.
- 25 Cassiani, M., Vinuesa, J.F., Galmarini, S., and Denby, B.: Stochastic fields method for  
26 sub-grid scale emission heterogeneity in mesoscale atmospheric dispersion models,  
27 *Atmos. Chem. Phys.*, 10, 267-277, 2010.
- 28 Ching, J.K.S., and Majeed, M.A.: An approach to characterized within-grid  
29 concentration variability in air quality models, *Atmos. Environ.*, 49, 348-360, 2012.

1 Ching, J.K.S.: A perspective on urban canopy layer modeling for weather, climate and  
2 air quality applications, *Urban Climate*, 3, 13-39, 2013.

3 CMAQ: Technical Documentation, Available at :  
4 [http://www.airqualitymodeling.org/cmaqwiki/index.php?title=CMAQ\\_version\\_5.0\\_%2](http://www.airqualitymodeling.org/cmaqwiki/index.php?title=CMAQ_version_5.0_%28February_2012_release%29_Technical_Documentation)  
5 [8February\\_2012\\_release%29\\_Technical\\_Documentation](http://www.airqualitymodeling.org/cmaqwiki/index.php?title=CMAQ_version_5.0_%28February_2012_release%29_Technical_Documentation), last access 8 January 2014.

6 Colette, A., Bessagnet, B., Meleux, F., Terrenoire, E., and Rouil, L.: Frontiers in air  
7 quality modelling, *Geosci. Model Dev.*, 7, 203-210, 2014.

8 Cuvelier, C., Thunis, P., Karam, D., Schaap, M., Hendriks, C., Kranenburg, R., Fagerli,  
9 H., Nyíri, Á., Simpson, D., Wind, P., Schulz, M., Bessagnet, B., Colette, A., Terrenoire,  
10 E., Rouil, L., Stern, R., Graff, A., Baldasano, J. M., and Pay, M. T.: ScaleDep:  
11 performance of European chemistry-transport models as function of horizontal spatial  
12 resolution, EMEP Report 1/2013, 63 pp., available at:  
13 [http://emep.int/publ/reports/2013/MSCW\\_technical\\_1\\_2013.pdf](http://emep.int/publ/reports/2013/MSCW_technical_1_2013.pdf), last access 4 April  
14 2013. Cohan, D.S., Hu, Y., and Russel, A.G.: Dependence of ozone sensitivity analysis  
15 on grid resolution, *Atmos. Environ.*, 40, 126-135, 2006.

16 Eder, B., Kang, D., Mathur, R., Yu, S., and Schere, K.: An operational evaluation of the  
17 Eta-CMAQ air quality forecast model, *Atmos. Environ.*, 40, 4894-4905, 2006.

18 EEA: CLC2006 technical guidelines. EEA Technical Report 17/2007. ISBN 978-90-  
19 9167-968-3. doi 10.2800/12134, 70 pp., 2007.

20 EEA: The application of models under the European Union's Air Quality Directive: A  
21 technical reference guide, EEA Technical report 10/2011, Publication Office of the  
22 European Union, Luxembourg, ISSN Technical report series 1725-2237, ISBN 978-92-  
23 9213-223-1, doi: 10.2800/80600, 76 pp., 2011.

24 EEA: Air quality in Europe- 2013 report, EEA Report 9/2013, ISSN 1725-9177, 112  
25 pp., 2013.

26 Fay, B. and Neunhäuserer, L.: Evaluation of high-resolution forecast with the non-  
27 hydrostatic numerical weather prediction model Lokal modell for urban air pollution  
28 episodes in Helsinki, Oslo and Valencia, *Atmos. Chem. Phys.*, 6, 2107-2128, 2006.

1 Fountoukis, C., Koraj, Dh., Denier van der Gon, H.A.C., Charalampidis, P.E., Pilinis,  
2 C., and Pandis, S.N.: Impact of grid resolution on the predicted fine PM by a regional 3-  
3 D chemical transport model. *Atmos. Environ.*, 68, 24-32, 2013.

4 Galmarini, S., Vinuesa, J.F., and Martilli, A.: Modeling the impact of sub-grid scale  
5 emission variability on upper-air concentration, *Atmos. Chem. Phys.* 8, 141-158, 2008.

6 Garber, W., Colosio, J., Grittner, S., Larssen, S., Rasse, D., Schneider, J. and Houssiau,  
7 M.: Guidance on the Annexes to Decision 97/101/EC on Exchange of Information as  
8 revised by Decision 2001/752/EC, Technical Report, European Commission, DG  
9 Environment, 2002.

10 García-Valero, J.A., Montávez, J.P., Jérez, S., Gómez-Navarro, J.J., Lorente-Plazas, R.,  
11 and Jiménez-Guerrero, P.: A seasonal study of the atmospheric dynamics over the  
12 Iberian Peninsula based on circulation types, *Theor. Appl. Climatol.*, 110, 219-310,  
13 2012.

14 Gego, E., Hogrefe, C., Kallos, G., Voudouri, A., Irwin, J., and Rao, S.T.: Examination  
15 of model predictions at different horizontal grid resolutions, *Environ. Fluid Mech.*, 5,  
16 63-85, 2005.

17 Gong, S.L.: A parameterization of sea-salt aerosol source function for sub- and super-  
18 micron particles, *J. Geophys. Res.*, 17, 197, 2003.

19 Guenther, A., Karl, T., Harley, P., Wiedinmyer, C., Palmer, P.I., and Geron, C.: 2006.  
20 Estimates of global terrestrial isoprene emissions using MEGAN (Model of Emissions  
21 of Gases and Aerosols from Nature), *Atmos. Chem. Phys.*, 6, 3181-3210, 2006.

22 Gonçalves, M., Jiménez-Guerrero, P., and Baldasano, J.M.: Contribution of atmospheric  
23 processes affecting the dynamics of air pollution in South-Western Europe during a  
24 typical summertime photochemical episode, *Atmos. Chem. Phys.*, 9, 849-864, 2009.

25 Guevara, M., Martínez, F., Arévalo, G., Gassó, S. and Baldasano, J.M.: An improved  
26 system for modelling Spanish emissions: HERMESv2.0, *Atmos. Environ.*, 81, 209-221,  
27 2013.

28 Jiménez, P., Jorba, O., Parra, R., and Baldasano, J.M.: Evaluation of MM5-  
29 EMICAT2002-CMAQ performance and sensitivity in complex terrains: High-resolution

1 application to the northeastern Iberian Peninsula, *Atmos. Environ.*, 40, 5056-5072,  
2 2006.

3 Kain, J.S. and Fritsch, J.M.: A one-dimensional entraining/detraining plume model and  
4 its application in convective parameterization, *J. Atmos. Sci.*, 47 (23), 2784-2802, 1990.

5 Kang, D., Eder, B.K., Stein, A.F., Grell, G.A., Peckham, S.E., and McHenry, J.: The  
6 new England air quality forecasting pilot program: development of an evaluation  
7 protocol and performance benchmark, *J. Air Waste Manage. Assoc.*, 55, 1782-1796,  
8 2005.

9 Kim, Y., Sartelet, K., Raut, Jean-Christophe, and Chazette, P.: Evaluation of the  
10 weather research and forecast/urban model over Greater Paris, *Boundary-Layer  
11 Meteorol.*, 149(1), 105-132, 2013.

12 Makar, P. A., Gravel, S., Chirkov, V., Strawbridge, K. B., Froude, F., Arnold, J., and  
13 Brook, J.: Heat flux, urban properties, and regional weather, *Atmos. Environ.*, 40,  
14 2750–2766, 2006.

15 Mathur, R., Shankar, U., Hanna, A.F., Odman, M.T., McHenry, J.N., Coats, C. J.,  
16 Alapaty, K., Xiu, A., Arunachalam, S., Olerud Jr., D. T., Byun, D. W., Schere, K. L.,  
17 Binkowski, F. S., Ching, J. K. S., Dennis, R. L., Pierce, T. E., Pleim, J. E., Roselle, S.  
18 J., and Young, J. O.: Multiscale Air Quality Simulation Platform (MAQSIP): Initial  
19 applications and performance for tropospheric ozone and particulate matter, *J. Geophys.  
20 Res.*, 110 (D13308), doi:10.1029/2004JD004918, 2005.

21 Mass, C., Ovens, D., Albright, M., and Westrick, K.: Does increasing Horizontal  
22 resolution Produce better Forecasts? The results of two years of Real-time Numerical  
23 Weather prediction in the Pacific Northwest, *B. Am. Meteorol. Soc.*, 83, 407-430, 2002.

24 Millán, M., Salvador, R., Mantilla, E., and Kallos, G.: Photooxidant dynamics in the  
25 Mediterranean basin in summer: results from European research projects, *J. Geophys.  
26 Res.*, 102, 8811– 8823, 1997.

27 Pay, M.T., Jiménez-Guerrero, P., and Baldasano, J.M.: Implementation of resuspension  
28 from paved roads for the improvement of CALIOPE air quality system in Spain, *Atmos.  
29 Environ.*, 45, 802-807, 2011.

1 Pay, M.T., Jiménez-Guerrero, P., Jorba, O., Basart, S., Pandolfi, M., Querol, X., and  
2 Baldasano, J.M.: Spatio-temporal variability of levels and speciation of particulate  
3 matter across Spain in the CALIOPE modeling system, *Atmos. Environ.*, 46, 376-396,  
4 2012a.

5 Pay, M. T., Gassó, S., and Baldasano, J.M.: Evaluation of the CMAQ5.0 in the  
6 framework of the CALIOPE air quality forecasting system over Europe, in: 11<sup>th</sup> Annual  
7 CMAS Conference, Chapel Hill, North Carolina, USA, 15-17 October 2012, 2012b.

8 Pérez, C., Nickovic, S., Baldasano, J.M., Sicard, M., Rocadenbosch, F., and Cachorro,  
9 V.E.: A long Saharan dust event over the western mediterranean: Lidar, sun photometer  
10 observations, and regional dust modeling, *J. Geophys. Res.* 111 (D15214), 1-16, 2006.

11 Pineda, N., Jorba, O., Jorge, J., and Baldasano, J.M.: Using NOAA AVHRR and SPOT  
12 VGT data to estimate surface parameters: application to a mesoscale meteorological  
13 model, *Int. J. Remote Sens.* 25, 129–143, 2004.

14 Queen, A. and Zhang, Y.: Examining the sensitivity of MM5-CMAQ predictions to  
15 explicit microphysics schemes and horizontal grid resolutions, Part III - the impact of  
16 horizontal grid resolution, *Atmos. Environ.*, 42, 3869-3881, 2008.

17 San José, R., Pérez, J.L., Morant, J.L., and González Barras, R.M.: The use of Modern  
18 third-generation air quality models (MM5-EMIMO-CMAQ) for real-time operational  
19 air quality impact assessment of industrial plants, *Water Air Soil Pollu.*, 9, 27-37, 2009.

20 Skamarock, W.C., and Klemp, J.B.: A time-split nonhydrostatic atmospheric model for  
21 weather research and forecasting applications, *J. Comput. Phys.* 227 (7), 3465-3485,  
22 doi:10.1016/j.jcp.2007.01.037, 2008.

23 Szopa, S., Foret, G., Menut, L., and Cozic, A.: Impact of large scale circulation on  
24 European summer surface ozone and consequences for modelling forecast, *Atmos.*  
25 *Environ.*, 43, 1189-1195, 2009.

26 Thompson, T.M., Saari, R.K., and Selin, N.E.: Air quality resolution for health impacts  
27 assessment: influence of regional characteristics, *Atmos. Chem. Phys. Discuss.*, 13,  
28 14141-14161, doi:10.5194/acpd-13-14141-2013, 2013.



1 Tesche, T.W., Morris, R., Tonnesen, G., McNally, D., Boylan, J., and Brewer, P.:  
2 CMAQ/CAMx annual 2002 performance evaluation over the eastern US, *Atmos.*  
3 *Environ.* 40, 4906-4919, 2006.

4 Timmermans, R.M.A., Denier van der Gon, H.A.C., Kuenen, J.J.P., Segers, A.J.,  
5 Honoré, C., Perrussel, O., Builtjes, P.J.H., and Schaap, M.: Quantification of the urban  
6 air pollution increment and its dependency on the use of down-scaled and bottom-up  
7 city emission inventories, *Urban Climate*, 6, 44-62, 2013.

8 Toll, I. and Baldasano, J. M.: Modeling of photochemical air pollution in the Barcelona  
9 area with highly disaggregated anthropogenic and biogenic emissions, *Atmos. Environ.*,  
10 34, 3060– 3084, 2000.

11 Valari, M. and Menut, L.: Does an increase in air quality models' resolution bring  
12 surface ozone concentrations closer to reality?, *J. Atmos. Oceanic Technol.*, 25, 1955-  
13 1968, 2008.

14 Valverde, V. V., Pay, M. T., and Baldasano, J. M.: Climatic synoptic classification over  
15 the Iberian Peninsula oriented to air quality dynamic characterization, *Int. J. Climatol.*,  
16 submitted, 2014.

17 Vivanco, M., Correa, M., Azula, O., Palomino, I., and Martín, F.: Influence of model  
18 resolution on ozone predictions over Madrid area (Spain), in: *Computational Science*  
19 *and Its Applications–ICCSA 2008* (pp. 165-178), Springer Berlin Heidelberg, 2008.

20 WHO: Review of evidence on health aspects of air pollution – REVIHAAP Project  
21 Technical report, World Health Organization, Regional Office for Europe, Copenhagen,  
22 Denmark, 2013.

23 Yarwood, G., Roa, S., Yocke, M., and Whitten, G.: Updates to the carbon bond  
24 chemical mechanism: CB05, Final report to the US EPA, RT-0400675, 2005.

25 Zhang, K., Knipping, E., Wexler, A., Bhave, P., and Tonnensen, G.: Size distribution of  
26 sea-salt emissions as a function of relative humidity, *Atmos. Environ.*, 39, 3373-3379,  
27 2005.

1 Zhang, Y., Bocquet, M., Mallet, V., Seigneur, C., and Baklanov, A.: Real-time air  
2 quality forecasting, part I: History, techniques, and current status, *Atmos. Environ.*, 60,  
3 632-655, 2012.

4

1 Table 1. CALIOPE-AQFS computational requirements, in terms of Central Processor  
 2 Units (CPU) and computational time (in min), for simulating 48h air quality forecasts as  
 3 a function of the domain: IP-4km (D2), AND-1km (D3), BCN-1km (D5) and MAD-  
 4 1km (D4), all of which are described in [Figure 1](#). D-domains are described in Figure 1.

	IP-4km (399x399 cells)	AND-1km (366x358 cells)	BCN-1km (146x146 cells)	MAD-1km (146x158 cells)
Meteorological Modeling	128 CPU/15 min	256 CPU/80 min	128 CPU/20 min	128 CPU/20 min
Emission Modeling	1 CPU/ 4 min	1 CPU/ 4 min	1 CPU/1 min	1 CPU/1 min
Air Quality modeling	256 CPU/210 min	256 CPU/220 min	128 CPU/150 min	128 CPU/110 min

5

6

1 Table 2. Discrete and categorical statistics for NO<sub>2</sub>, O<sub>3</sub>, O<sub>3</sub>-8h, and PM<sub>10</sub> for April 2013  
 2 as a function of horizontal resolution (4 km and 1 km). n indicates the number of pairs  
 3 of data used in the discrete evaluation on an hourly basis. OM and MM depict the  
 4 measured and modeled mean concentrations, respectively. T is the threshold applied in  
 5 the categorical evaluation. Max 1h and mean 24h concentrations are calculated by  
 6 considering  $\geq 75\%$  of the hours in a day, as established by Directive 2008/50/EC.

	NO <sub>2</sub>	O <sub>3</sub>	O <sub>3</sub> -8h	PM <sub>10</sub>
n (stations)	90761 (135)	76471 (114)	3248 (114)	66642 (100)
OM ( $\mu\text{gm}^{-3}$ )	22.0	68.4	88.6	20.6
EU LV/TV ( $\mu\text{gm}^{-3}$ ) (temp basis)	200 (Max 1h)	180 (Max 1h)	120 (Max 8h)	50 (Mean 24h)
EU LV/TV exceedances	0	25	0	31
T* ( $\mu\text{gm}^{-3}$ ) (temp. basis)	71 (Max 1h)	108 (Max 1h)	101 (Max 8h)	27 (Mean 24h)

Discrete evaluation

	4 km	1 km	4 km	1 km	4 km	1 km	4 km	1 km
MM ( $\mu\text{gm}^{-3}$ )	17.4	19.3	58.0	57.3	72.4	71.5	13.9	14.0
r	0.54	0.54	0.61	0.61	0.54	0.51	0.45	0.44
MB ( $\mu\text{gm}^{-3}$ )	-4.5	-2.6	-10.5	-11.3	-16.3	-17.2	-6.7	-6.6
MAE ( $\mu\text{gm}^{-3}$ )	12.9	13.2	19.7	19.8	18.4	19.2	12.6	12.7
RMSE ( $\mu\text{gm}^{-3}$ )	19.8	20.4	24.6	24.7	21.8	22.8	17.2	17.4
MNBE (%)	-20.4	-11.8	-15.3	-16.5	-18.4	-19.4	-32.5	-32.0
MNGE (%)	58.5	59.9	28.8	28.9	20.8	21.7	61.1	61.6
MFB (%)	-28.5	-23	-13.1	-15.1	-19.3	-20.5	-63.3	-64.1
MFE (%)	69.2	68.7	37.1	37.4	22.5	23.5	85.7	87.1

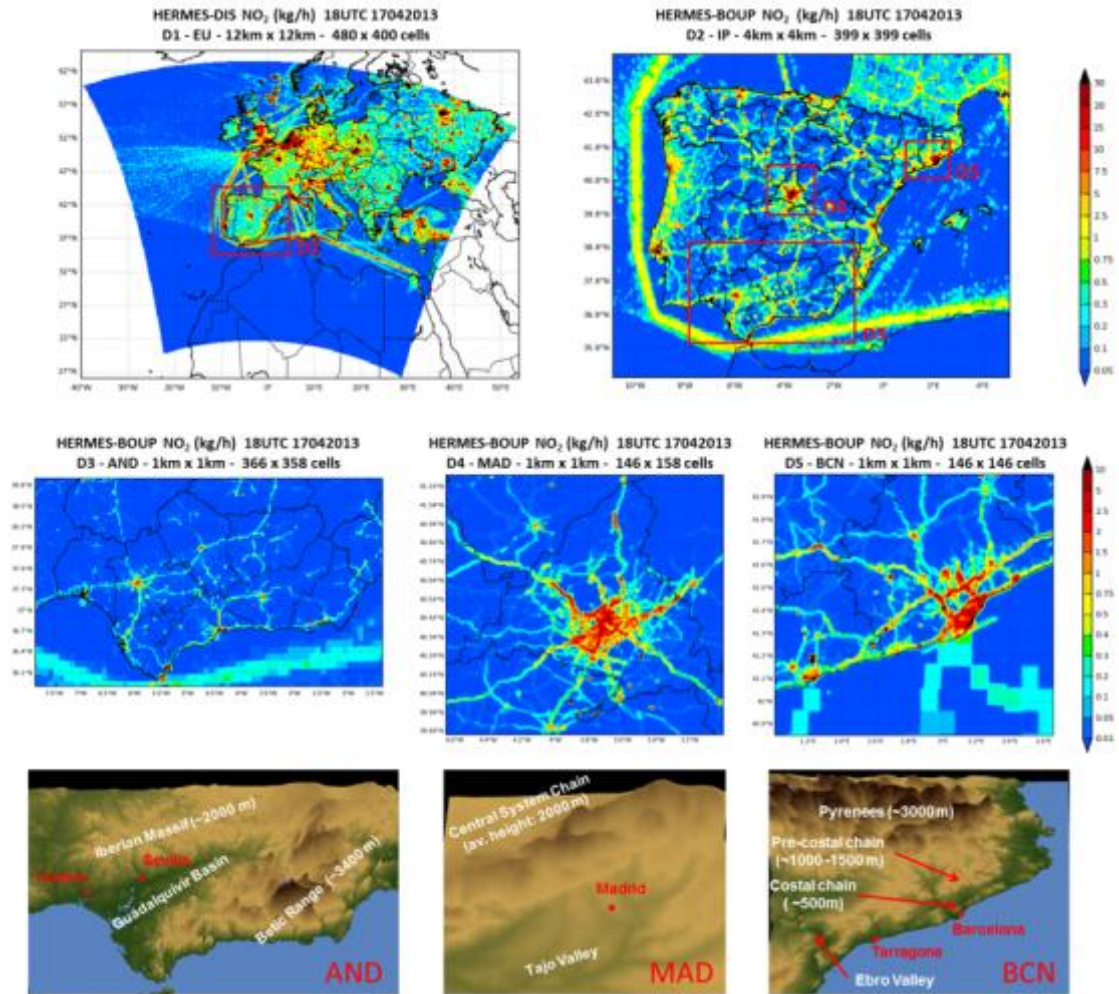
Categorical evaluation (Threshold = T\*)

	4 km	1 km	4 km	1 km	4 km	1 km	4 km	1 km
a (false alarm)	306	384	41	19	17	6	131	133
b (hits)	466	537	112	96	6	4	331	334
c (correct negative)	2517	2439	1846	1868	2826	2837	1978	1976
d (misses)	487	416	1194	1210	399	401	334	331
B (% , 100)	37	40	8	7	1	1	42	42
POD (% , 100)	49	56	9	7	1	1	50	50
CSI (% , 100)	81	97	12	9	6	2	69	70
FAR (% , 0)	40	42	27	17	74	60	28	28
A (% , 100)	79	79	61	62	87	87	83	83

T\* is defined as 75p of the observed concentrations estimated temporally, as established by EU Directive 2008/50/EC

7

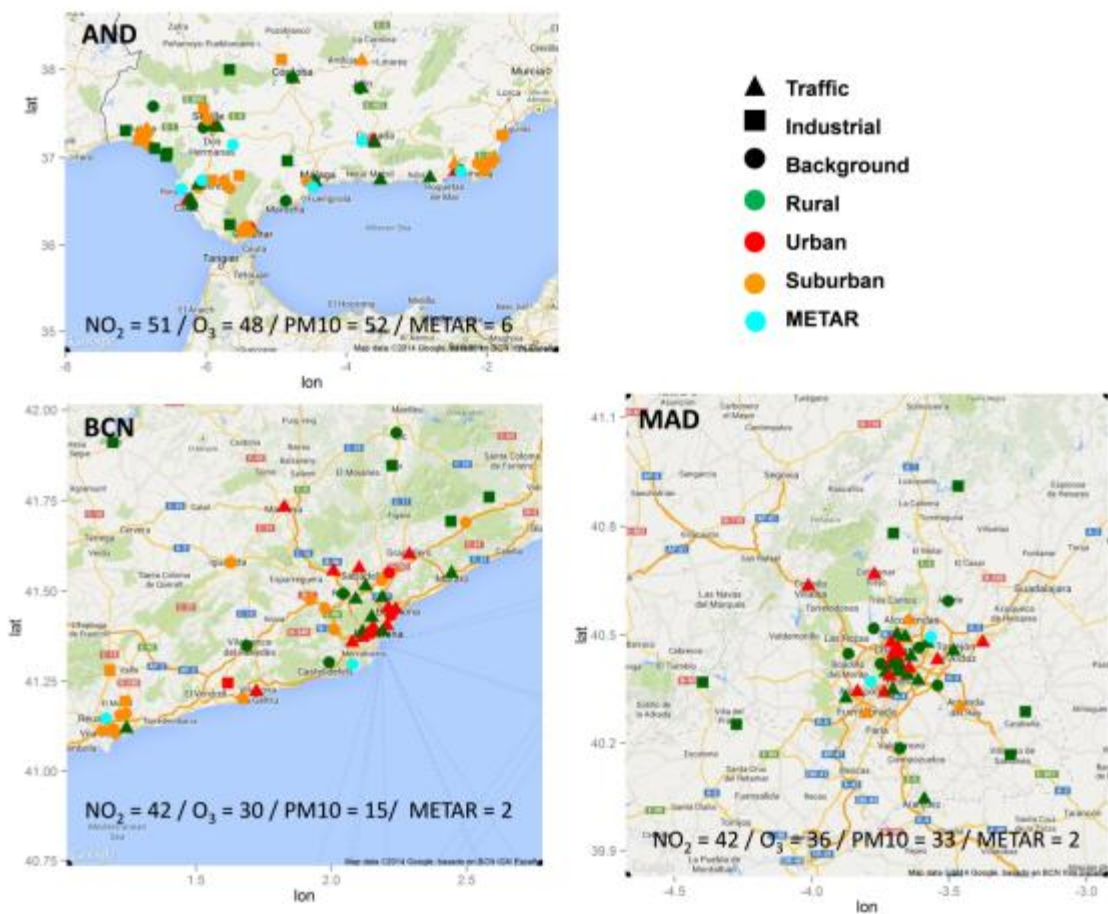
8



1

2 Fig. 1. CALIOPE-AQFS nesting strategy (D-domains) and study domains (Andalucia,  
3 AND; Madrid, MAD; and Barcelona, BCN). Colour chart at D-domains shows NO<sub>2</sub>  
4 emission rate (kg h<sup>-1</sup>) for 17<sup>th</sup> April, 2013 at 18UTC. HERMES-DIS model generates  
5 emissions at 12 km x 12 km over Europe (the mother domain, D1) by performing  
6 disaggregation from the EMEP database. HERMES-BOUP model estimates emissions  
7 at 1 km x 1 km, following a bottom-up approach.

8

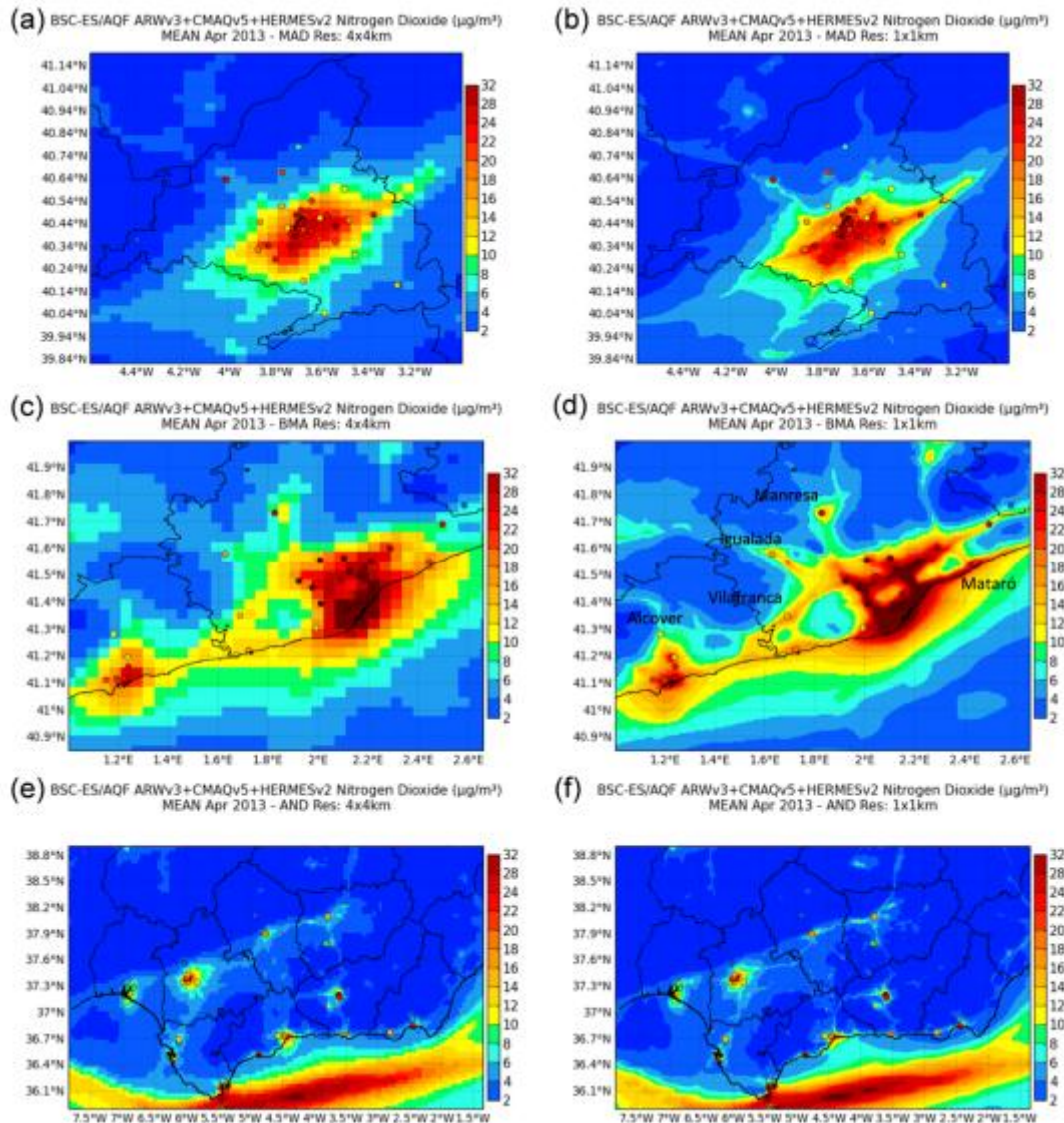


1

2 Figure 2. Air quality stations for  $\text{NO}_2$ ,  $\text{O}_3$  and  $\text{PM}_{10}$  in the three domains under study  
 3 (AND, BCN and MAD) in April 2013. Different types of stations are shown by symbols  
 4 and color codes. The various symbols represent the major emission type affecting each  
 5 station (Traffic: triangle; Industrial: square; and Background: circle), while the colors  
 6 reflect the environment of each station (Urban: red; Suburban: green; and Rural:  
 7 orange). Cyan dots represent METAR stations used in Sect. S1.

8

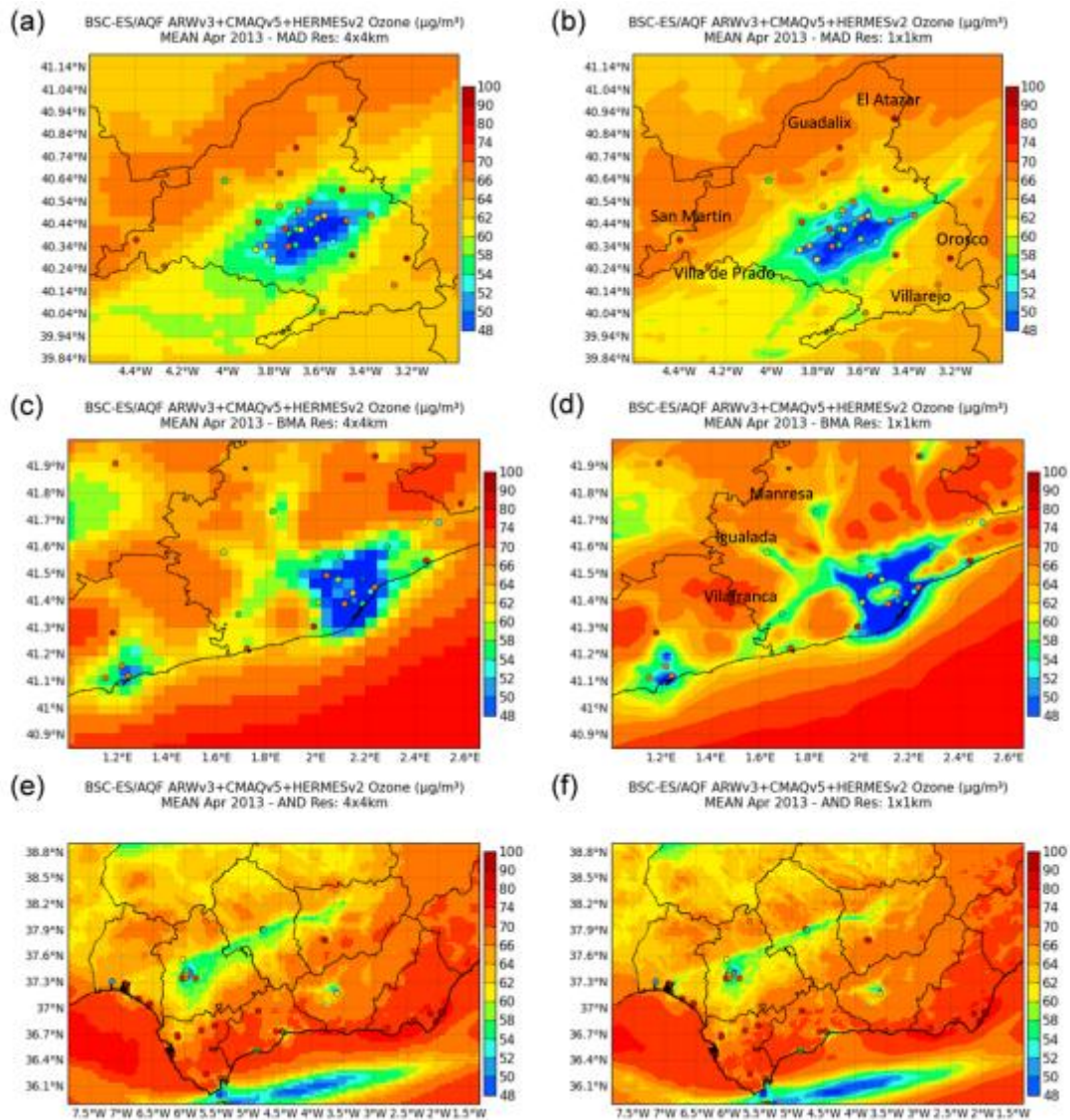




1

2 Figure 3. CALIOPE-AQFS mean NO<sub>2</sub> concentration (µg/m<sup>3</sup>) in April 2013 over (a,b)  
 3 MAD, (c,d) BCN, and (e,f) AND, as a function of horizontal resolution: 4 km (left  
 4 column) and 1 km (right column). Dots indicate mean concentration at air quality  
 5 stations.

6

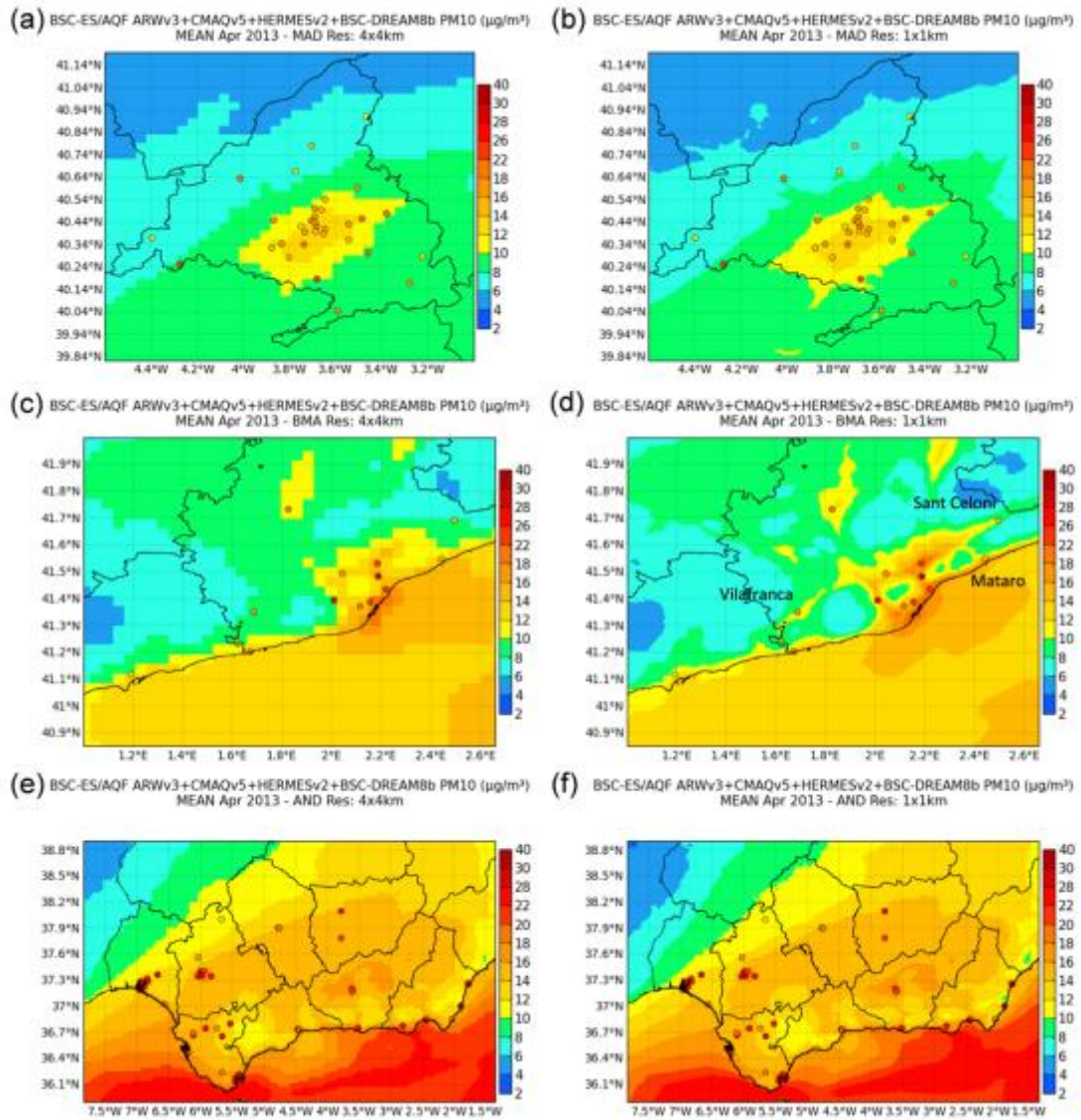


1

2 Figure 4. CALIOPE-AQFS mean O<sub>3</sub> concentration (µg m<sup>-3</sup>) in April 2013 over (a,b)  
 3 MAD, (c,d) BCN, and (e,f) AND, as a function of horizontal resolution: 4 km (left  
 4 column) and 1 km (right column). Dots indicate mean concentration at air quality  
 5 stations.

6

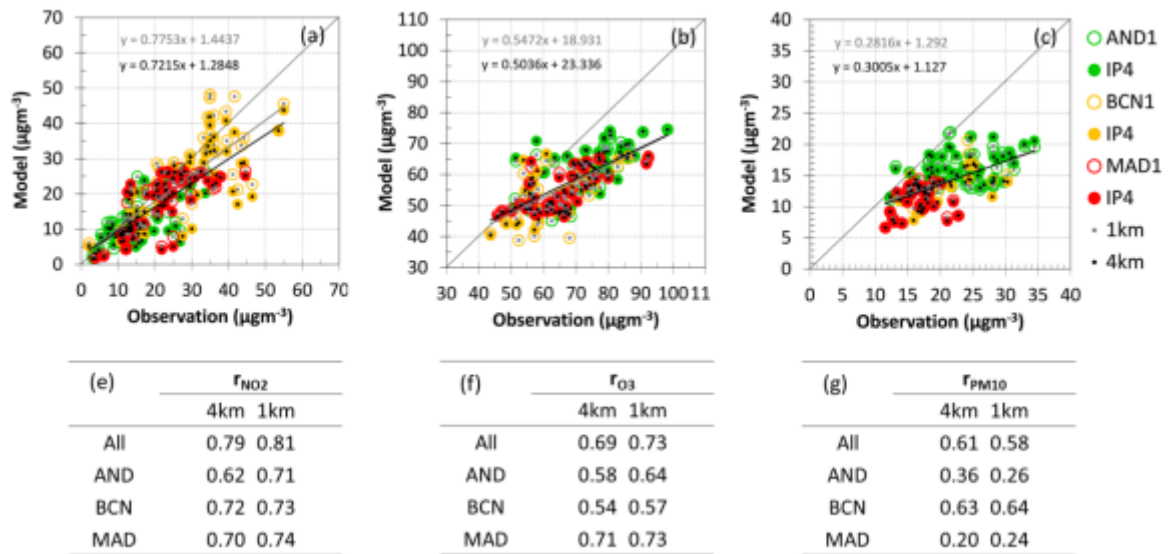




1

2 Figure 5. CALIOPE-AQFS mean  $\text{PM}_{10}$  concentration ( $\mu\text{g}/\text{m}^3$ ) in April 2013 over (a,b)  
 3 MAD, (c,d) BCN, and (e,f) AND, as a function of horizontal resolution: 4 km (left  
 4 column) and 1 km (right column). Dots indicate mean concentrations at air quality  
 5 stations.

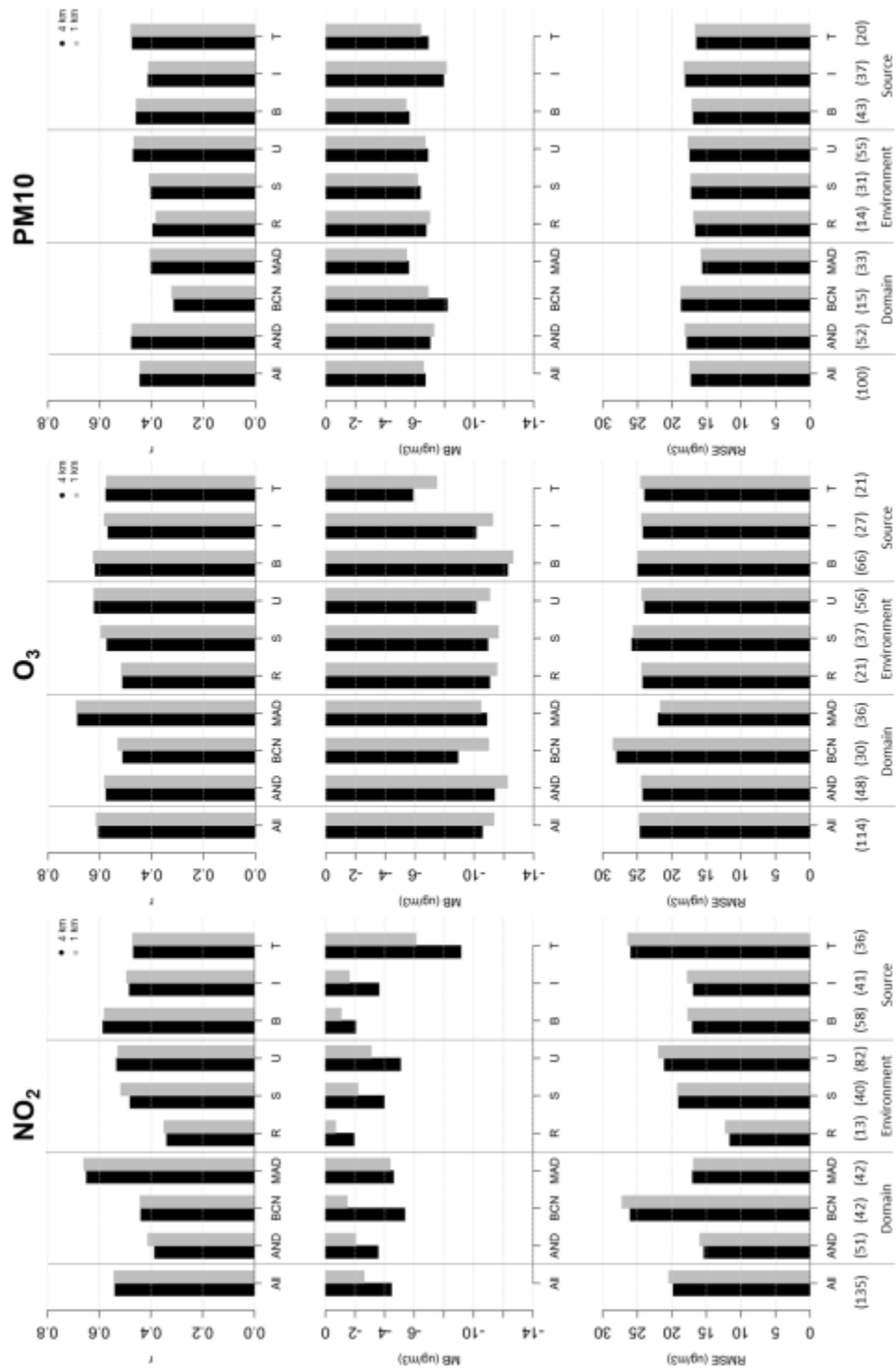
6



1

2 Figure 6. Monthly mean scatter plots for CALIOPE-AQFS (y-axis) and observed (x-  
 3 axis) concentrations for the three study domains (AND in green, BCN in yellow, and  
 4 MAD in red), as a function of horizontal resolution for (a) NO<sub>2</sub>, (b) O<sub>3</sub> and (c) PM<sub>10</sub>.  
 5 Equations show the linear adjustment between models and observations at 1 km (light  
 6 grey) and 4 km (dark grey). Spatial correlation coefficients as a function of resolution  
 7 and domain are shown for (e) NO<sub>2</sub>, (f) O<sub>3</sub>, and (g) PM<sub>10</sub>.

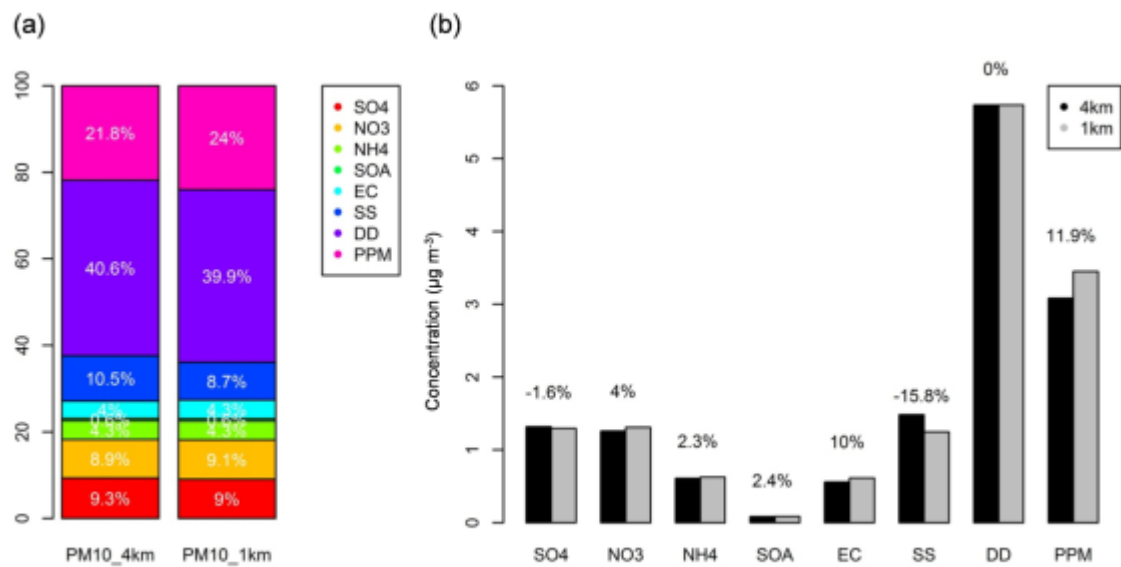
8



1

2 Figure 7. Statistics (r, MB, and RMSE in rows) for each pollutant ( $\text{NO}_2$ ,  $\text{O}_3$ , and  $\text{PM}_{10}$ )  
 3 in columns) on an hourly basis as a function of horizontal resolution: 4 km (black) and 1  
 4 km (grey). Four categories are considered: all stations (all), domain (AND, BCN and  
 5 MAD), station environment (R, S, and U), and main sources (B, I, and T).

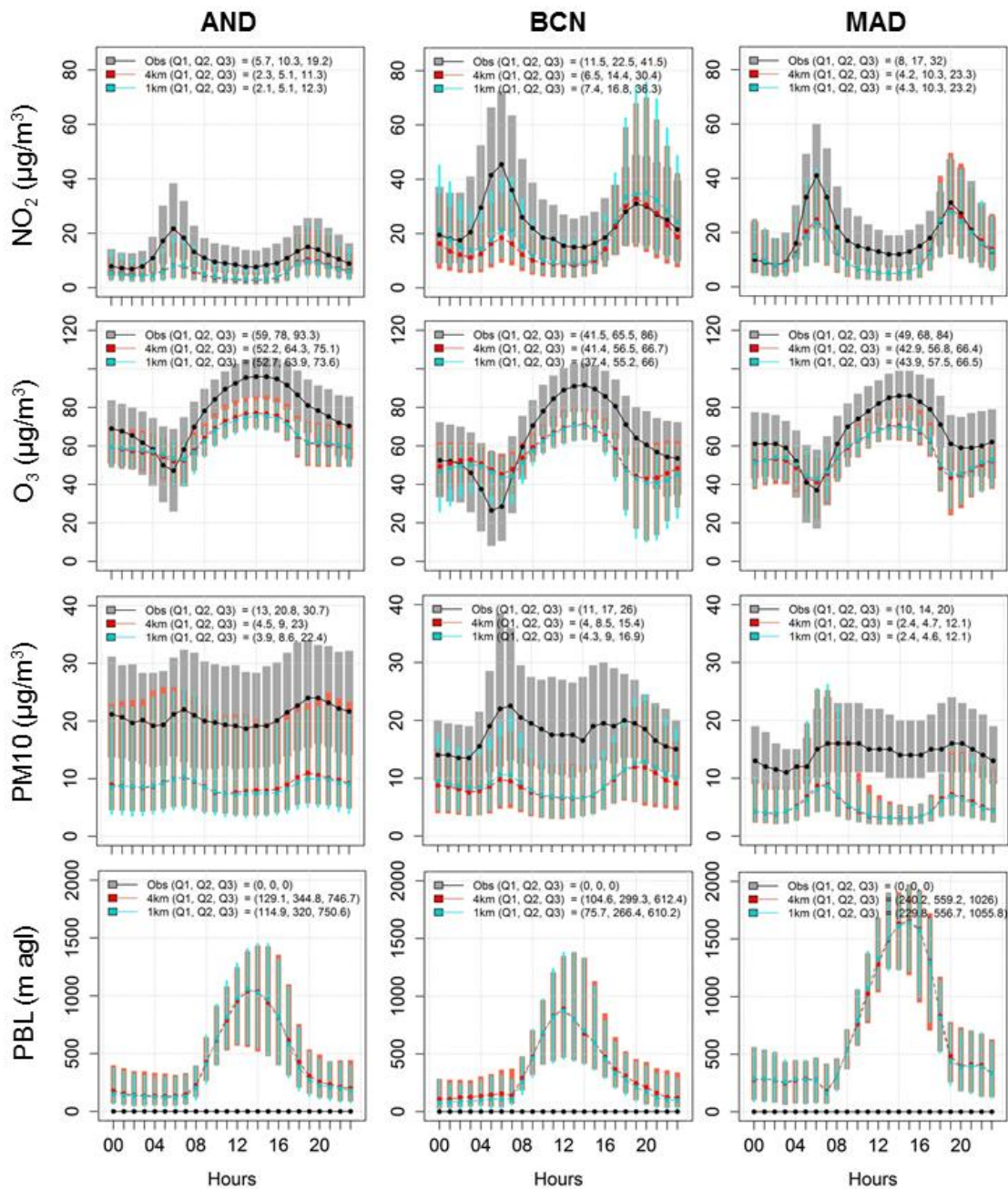
6



1

2 Figure 8. Resolution effect on PM<sub>10</sub> components in April 2013. (a) Percentage of PM<sub>10</sub>  
 3 components: sulfate (SO<sub>4</sub>), nitrate (NO<sub>3</sub>), ammonium (NH<sub>4</sub>), secondary organic  
 4 aerosol (SOA), elemental carbon (EC), sea salt (SS), desert dust (DD), and primary  
 5 particulate matter (PPM). (b) PM<sub>10</sub> component concentrations in the 1-km simulation  
 6 (black) and 4-km simulation (grey). Numbers over bars indicate the % of increase when  
 7 increasing resolution.

8

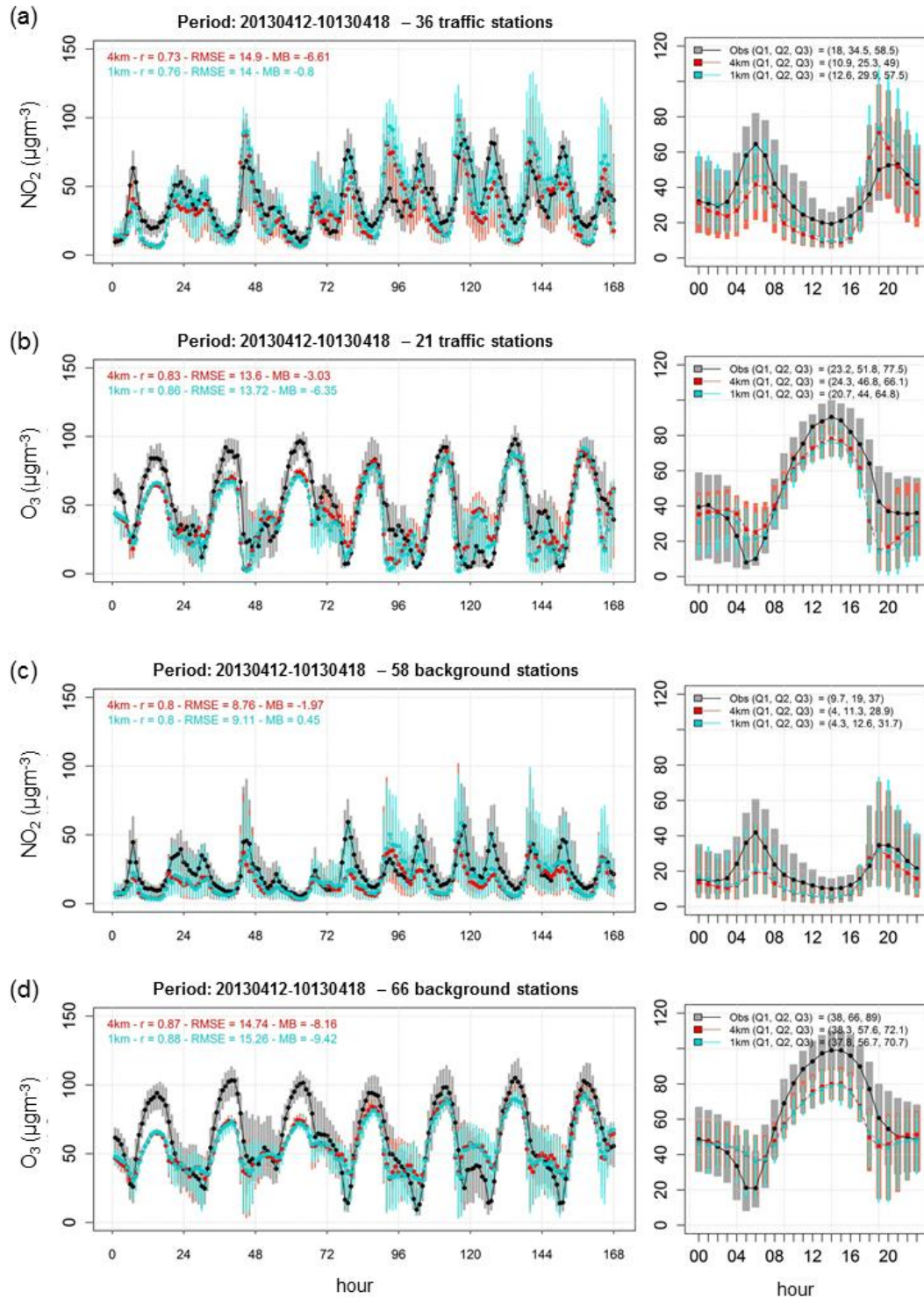


1

2 Figure 9. Daily cycles for  $\text{NO}_2$ ,  $\text{O}_3$  and  $\text{PM}_{10}$  for each study domain at available stations  
 3 as a function of resolution. No observations of PBL are available. Q1, Q2 and Q3  
 4 indicate quartiles for the daily cycle. Bars show Q1 and Q3 at each hour.

5





1

2 Figure 10. Temporal series and daily cycles for NO<sub>2</sub> and O<sub>3</sub> at background (a and b,  
 3 respectively) and traffic stations (c and d, respectively) for the episode of 12-18<sup>th</sup> April,  
 4 2013. Q1, Q2 and Q3 indicate quartiles for the daily cycle. Bars show Q1 and Q3 at  
 5 each hour.